Published in final edited form as:
Neuron. 2021 October 20; 109(20): 3283–3297.e11. doi:10.1016/j.neuron.2021.10.001.

A synaptic temperature sensor for body cooling

Gretel B. Kamm[#1], **Juan C. Boffi**[#1,2,6], **Kristina Zuza**[1], **Sara Nencini**[1], **Joaquin Campos**[3], **Katrin Schrenk-Siemens**[1], **Ivo Sonntag**[2], **Burce Kabaoğlu**[1], **Muad Y. Abd El Hay**[1], **Yvonne Schwarz**[4], **Anke Tappe-Theodor**[1], **Dieter Bruns**[4], **Claudio Acuna**[3], **Thomas Kuner**[2], **Jan Siemens**[1,5,8,*]

[1]Department of Pharmacology, University of Heidelberg, Im Neuenheimer Feld 366, 69120 Heidelberg, Germany

[2]Department of Functional Neuroanatomy, Institute for Anatomy and Cell Biology, University of Heidelberg, Im Neuenheimer Feld 307, 69120 Heidelberg, Germany

[3]Chica and Heinz Schaller Foundation, Institute for Anatomy and Cell Biology, University of Heidelberg, Im Neuenheimer Feld 307, 69120 Heidelberg, Germany

[4]Institute for Physiology, Center of Integrative Physiology and Molecular Medicine, Saarland University, Homburg, Germany

[5]Molecular Medicine Partnership Unit (MMPU), European Molecular Biology Laboratory (EMBL), Meyerhofstraße 1, 69117 Heidelberg, Germany

[6]Present address: Cell Biology and Biophysics Unit, European Molecular Biology Laboratory (EMBL), Meyerhofstraße 1, 69117 Heidelberg, Germany

[#] These authors contributed equally to this work.

Summary

Deep brain temperature detection by hypothalamic warm-sensitive neurons (WSNs) has been proposed to provide feedback information relevant for thermoregulation. WSNs increase their action potential firing rates upon warming, a property that has been presumed to rely on the composition of thermosensitive ion channels within WSNs. Here, we describe a synaptic mechanism that regulates temperature sensitivity of preoptic WSNs and body temperature.

[*]Correspondence: jan.siemens@pharma.uni-heidelberg.de.
[8]Lead contact

Author Contributions

J.S. and G.B.K. conceived the project. G.B.K. built and established the thermodes, brain thermometers, thermic chamber, and voltage imaging and conducted all *in vivo* temperature and thermode experiments. I.S. built the Miniscopes and established GRIN lens implantations in the POA together with G.B.K. *In vivo* imaging data analysis was performed by I.S., G.B.K., and J. C.B. T.K. oversaw *in vivo* imaging and contributed to electrophysiological data analysis and interpretation. J.C.B. designed and performed electrophysiological experiments. G.B.K. and J.C.B. performed calcium imaging of presynaptic terminals in mouse brain slices. S.N., together with C.A., carried out the postsynaptic current recordings in brain slices and, together with K. Z., designed and performed electrophysiological synaptic blocker experiments, optogenetics, and calcium imaging of iPSC-derived neurons. Y.S. and D.B. performed synaptic recordings. J.C., C.A., and K.S.-S. designed all iPSC-derived neuron experiments, characterized the custom-made anti-TRPM2 antibody, and performed western blots and antibody stainings with B.K. M.Y.A.E.H. contributed to the analysis of calcium- and voltage-imaging data. G.B.K., together with A.T.-T., performed the sensory neuron ablation experiments and behavioral testing. J.S., together with G.B.K. and J.C.B., wrote the paper. All authors commented on and approved the paper.

Declaration Of Interests

The authors declare no competing interests.

Europe PMC Funders Author Manuscripts

Experimentally induced warming of the mouse hypothalamic preoptic area *in vivo* triggers body cooling. TRPM2 ion channels facilitate this homeostatic response and, at the cellular level, enhance temperature responses of WSNs, thereby linking WSN function with thermoregulation for the first time. Rather than acting within WSNs, we—unexpectedly—find TRPM2 to temperature-dependently increase synaptic drive onto WSNs by disinhibition. Our data emphasize a network-based interoceptive paradigm that likely plays a key role in encoding body temperature and that may facilitate integration of diverse inputs into thermoregulatory pathways.

Abstract

Europe PMC Funders Author Manuscripts

Europe PMC Funders Author Manuscripts

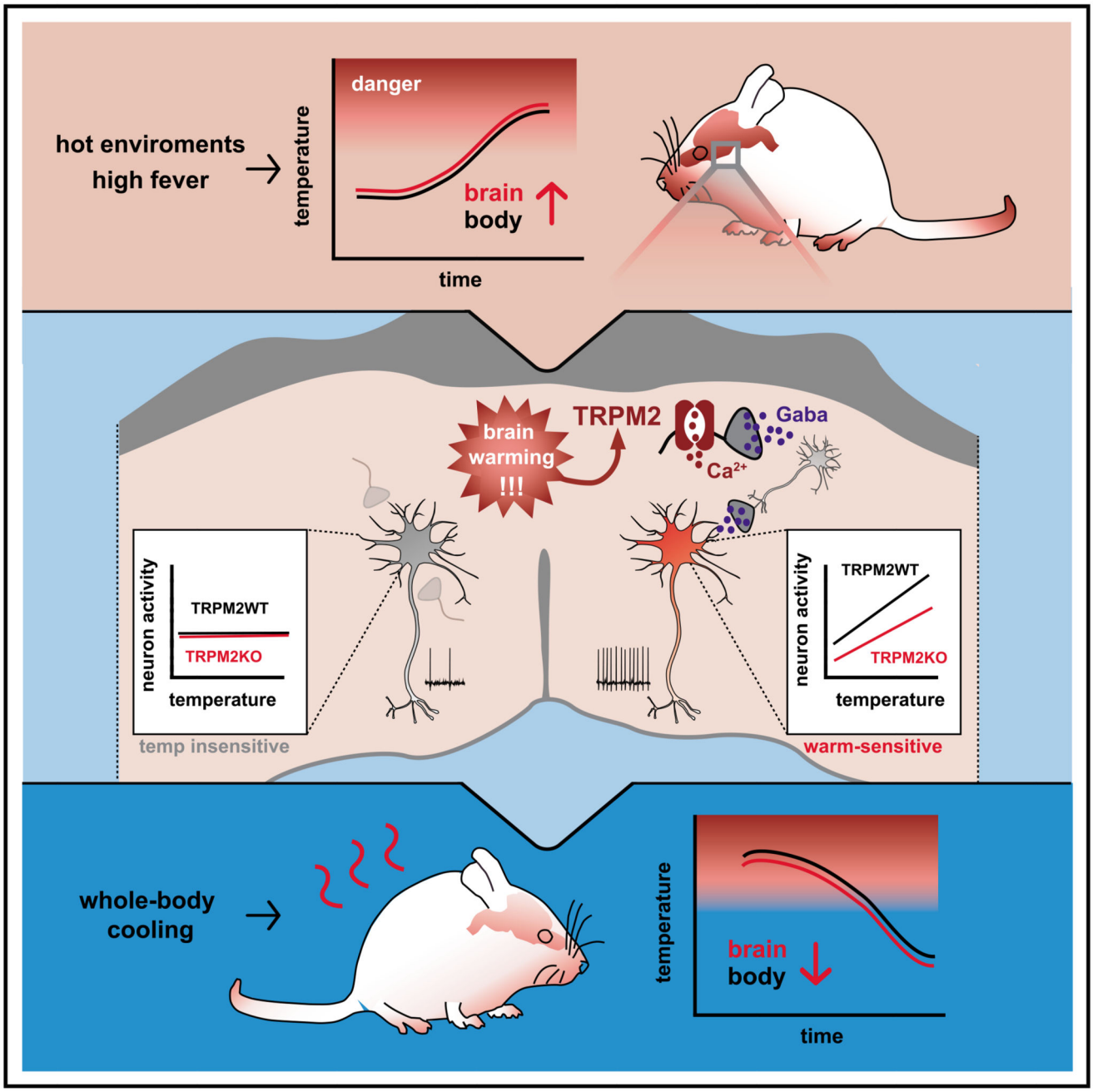

Graphical abstract.

Introduction

The hypothalamus is a central regulator of bodily homeostasis. To accomplish this task, this deep-seated brain structure has privileged access to capillary blood and blood-borne signaling molecules to detect and integrate interoceptive cues. Decades of research have shown that experimental warming of the anterior hypothalamus and preoptic area (POA)

triggers heat loss responses and body cooling (Barbour, 1912; Hammel, 1968; Heller et al., 1978; Magoun et al., 1938; Morrison and Nakamura, 2019; Siemens and Kamm, 2018; Tan and Knight, 2018). Detection of deep brain temperature increases have been attributed to the requisite role of intrinsically warm-sensitive neurons (WSNs). WSNs increase their action potential firing rates upon warming, a property that has been presumed to rely exclusively on the composition of thermosensitive ion channels within WSNs (Madden and Morrison, 2019). However, specific mechanisms mediating thermosensitivity in WSNs have remained elusive, rendering it impossible to assess WSN contribution to hypothalamic thermoregulation. Moreover, and given their deep brain location, the physiological relevance of preoptic temperature sensitivity has been questioned altogether (Tan et al., 2016).

Results

POA temperature tracks body temperature

We started by assessing whether deep brain temperature (TPOA) of the mouse fluctuates under physiological conditions—similar to body temperature (T_{core})—a prerequisite for POA warm sensitivity to be physiologically relevant. To simultaneously access TPOA and Tcore in freely moving mice, we implanted temperature probes into the POA and abdominal cavity, respectively (Figure 1A). Interestingly, T_{POA} precisely matched T_{core}: even minute fluctuations of T_{core} were recapitulated in T_{POA} (Figures 1B and S1A). Moreover, rapid changes in T_{core} triggered during fever and ambient heat stress increased TPOA and Tcore to similar levels (Figures S1B and S1C). At the opposite extreme, metabolic perturbation and obesity known to reduce T_{core} also reduced T_{POA} (Figure S1D). Overall, we find that T_{POA} tracks T_{core} with high fidelity (Figure 1C). Temperatures measured at the level of the neocortex (TCTX) were consistently lower compared to T_{POA} and T_{core} (Figures 1D and S1E-S1G), in agreement with previous models predicting (Sukstanskii and Yablonskiy, 2004) or measuring (Coman et al., 2013; Vishwakarma et al., 2020) temperature gradients across mammalian brains. We conclude that the POA is ideally positioned to detect body temperature changes, presumably due to its vicinity to peripherally tempered blood entering the brain via the internal carotid arteries and the Circle of Willis (Baker, 1979; Fenrich et al., 2021).

TRPM2 mediates hypothalamic temperature detection *in vivo*

We recently implicated TRPM2, a heat-sensitive member of the TRP ion channel family, in regulating fever and found that this ion channel mediates temperature responses in cultured POA neurons (Song et al., 2016). However, a role of TRPM2 in interoceptive, deep brain temperature sensing has previously not been established. To probe thermosensitivity of TRPM2 *in vivo,* we next aimed to locally change POA temperature in awake mice. Temperature stimulation of the POA was pioneered more than 80 years ago (Barbour, 1912; Magoun et al., 1938) and subsequently established in large animal models (Baldwin and Ingram, 1967; Hammel et al., 1960) inconvenient for genetic manipulation. Hence, we developed a miniature head-mounted temperature stimulator suitable for POA warming in freely moving, cable-tethered mice (Figure 2A; Video S1). The system, from here on referred to as thermode, was modeled according to a previous design used in songbirds (Long and Fee, 2008).

First, we assessed the magnitude of the warming effect that our thermode can achieve *in vivo*. We unilaterally heated the POA, while recording brain temperatures contralaterally with a thin thermocouple. The distance between the thermode and the thermocouple was measured post hoc using microcomputed tomography (micro-CT; Figure S1H). The thermode allowed us to generate a locally restricted warming stimulus across the POA with a maximum temperature of $\Delta T = 5°C$ at the center of the stimulation site and $\Delta T = 1°C$ measured on the contralateral side of the POA (Figures S1I–S1K).

Next, we warmed the POA in two steps, first to 39°C and subsequently further to 41°C, while simultaneously measuring body temperature (T_{core}) telemetrically. This stimulation paradigm resulted in homeostatic body cooling (Figure 2B).

Thermoregulatory responses declined with temperature stimulations performed more rostrally or more caudally (Figure S2A), suggesting that the central POA (approximately +0.50 and +0.01 Bregma) had the highest temperature sensitivity. Consequently, the central POA was targeted in all subsequent thermode stimulation experiments.

Longer stimulation at 41°C prolonged the hypothermic period beyond the stimulation phase and reduced ambulatory activity of the animals. This persistent decrease in T_{core} likely reflected a form of thermal plasticity (but not permanent tissue damage) because T_{core} recovered after several days (Figures S2B-S2D). Additionally, thermode-induced body cooling could be repeated several times, further supporting that the cooling response was not triggered by tissue damage (data not shown). Moreover, “genetically tagging” and reactivating neurons that had previously been excited by thermode stimulation (Figures 2C and 2D), using the Fos-TRAP2 mouse line (Allen et al., 2017), further supported response specificity. Chemogenetic activation of Gq-DREADD receptors (Roth, 2016) permissively expressed by Tamoxifen injection during thermode stimulation in the POA of Fos-TRAP2 mice was able to recapitulate the body-cooling response 2 weeks after thermode stimulation (Figure 2E). No significant chemogenetically activated body-cooling response was observed in thermode-implanted—but unstimulated—control animals (Figure 2E). These results demonstrate that a population of POA neurons, presumably WSNs, are activated by thermode stimulation to drive body cooling.

To assess whether TRPM2 is relevant for POA temperature sensitivity *in vivo,* we thermode-stimulated the POA of *Trpm2* knockout (*Trpm2*$^{-/-}$) mice (Yamamoto et al., 2008). Indeed, the homeostatic body-cooling response was significantly reduced in *Trpm2*$^{-/-}$ mice (Figure 3A). Furthermore, long-lasting reduction in body temperature that typically followed strong warming of the POA was absent in *Trpm2*$^{-/-}$ animals (Figures S2E and S2F). These results implicate TRPM2 in local POA temperature detection, relevant for T_{core} regulation.

POA warmth sensitivity in *Trpm2*$^{-/-}$ mice was reduced but not abolished. To assess whether preoptic Trpm2-expressing neurons (POA^{Trpm2} neurons) are more critically involved in deep brain temperature detection, we ablated thispopulation by viral delivery of Cre-dependent caspase-3 (Yang et al., 2013) into the POA of Trpm2-Cre mice (Song et al., 2016). Strikingly, deleting POA^{Trpm2} neurons essentially abolished homeostatic body cooling upon thermode-driven deep brain warming (Figures 3B, S3A, and S3B).

We noted, however, that Trpm2-Cre control mice in the absence of caspase-3 already had a partial deficit in body cooling (Figure 3B), similar to *Trpm2*$^{-/-}$ mice. We, therefore, wondered whether knocking in the Cre transgene into the *Trpm2* genomic locus compromised TRPM2 protein expression in heterozygous Trpm2-Cre mice, thereby explaining the reduced response. Indeed, western blotting using POA brain tissue revealed that TRPM2 protein levels were severely reduced in heterozygous Cre-positive mice when compared to Cre-negative littermate controls (Figure S3C). POA protein extracts of *Trpm2*$^{-/-}$ mice served as specificity control for the custom-made monoclonal anti-TRPM2 antibody. Collectively, these results demonstrate that POA$^{\text{Trpm2}}$ neurons are required for mounting a cooling response when deep brain temperature is on the verge of exceeding physiological levels, with the TRPM2 channel enhancing this thermoregulatory response.

TRPM3, a heat-pain sensor in the peripheral nervous system (Vandewauw et al., 2018; Vriens et al., 2011), is also found in the hypothalamus (Song et al., 2016) (Figure S3D). However, thermode stimulation of *Trpm3*$^{-/-}$ mice showed no significant difference in body cooling when compared to littermate controls (Figure S3E).

Other TRP channels have been implicated in detecting warmth and heat, most notably the capsaicin receptor TRPV1 (Caterina et al., 1997; Yarmolinsky et al., 2016). To further assess the specificity of preoptic TRPM2 in mediating deep brain temperature responses, we used Trpv1-Cre mice in combination with Cre-dependent diphtheria toxin expression to ablate Trpv1-expressing cells. This approach eliminates most, if not all, peripheral thermosensory neurons (Mishra et al., 2011; Pogorzala et al., 2013) (Figures S3F-S3H). Thermode stimulation did not reveal any thermoregulatory differences in Trpv1$^{\text{Abl}}$ versus non-ablated (Trpv1 $^{\text{wt}}$)animals (Figures S3I and S3J), suggesting that Trpv1-expressing—peripheral and central—neurons do not contribute significantly to warmth sensing in the POA.

TRPM2 expression does not demarcate WSNs

Temperature sensing in the POA has historically been attributed to the requisite and cell-autonomous role of WSNs, i.e., neurons that increase action potential (AP) firing in response to temperature increase (Madden and Morrison, 2019; Tan and Knight, 2018). The temperature coefficient (TC), the slope of AP rate versus temperature, has been used as the defining feature to categorize and quantify WSNs *in vivo* and in brain slice preparations (Boulant and Dean, 1986; Kelso etal., 1982; Kobayashi and Takahashi, 1993; Tabarean, 2018). Given that we found POA heat sensing to be reduced, but not abolished, in *Trpm2*$^{-/-}$ mice *in vivo*, we speculated that the absence of TRPM2 would alter WSN abundance. Thus, we subjected POA slices to a sinusoidal-shaped warming stimulus (Figure 4A) and applied a conservative and classically used TC lower limit of 0.8 Hz/°C (Boulant and Dean, 1986) to identify WSNs (Figures 4B and 4C). By randomly sampling POA neurons electrophysiologically using POA brain slices of wild-type and *Trpm2*$^{-/-}$ mice, we found similar fractions of WSNs in both genotypes (Figures 4D and 4E; 21% versus 27%, respectively; $p = 0.6$, chi-square test).

While this result was somewhat unexpected, it suggested that the TRPM2 channel does not influence WSN abundance and, hence, prompted us to record Trpm2-positive neurons (from

Trpm2-Cre mice), still assuming POA^{Trpm2} neurons to be WSNs. These recordings revealed that 18% of POA^{Trpm2} neurons are WSNs (16/88 neurons; Figure 4F). This low percentage is akin to that of $Trpm2^{Cre}$-negative neurons (23%) and randomly sampled WSNs recorded in POA slices obtained of *Trpm2*$^{+/+}$ and *Trpm2*$^{-/-}$ mice (Figure 4E), suggesting that WSNs are not enriched in the POA^{Trpm2} population.

To assess *in vivo* whether POA^{Trpm2} neurons demarcate WSNs and/or a population responding to ambient heat stimuli detected by the peripheral nervous system (so-called warm-responsive neurons [WRNs]; Siemens and Kamm, 2018), we subjected Trpm2-Cre animals to temperature challenges while simultaneously monitoring POA^{Trpm2} neuron activity by GCaMP6-based micro-endoscopic (Miniscope) imaging in freely moving mice (Ghosh et al., 2011) (Figure 4G).

While POA^{Trpm2} neurons are not excluded from the WRN population, we again found little overlap, with only 23% of POA^{Trpm2} neurons (48/210, n = 6 mice) contributing to the WRN population (Figures 4H and S4A-S4L). In 10% of neurons, we also observed a response to ambient cooling.

When subjecting mice to a constant heat stimulus with a maximum ambient temperature of $T_{amb} = 40 \pm 1°C$, we noted that the body temperature of the animals started to increase as a consequence of the long-lasting challenge (Figure 4H, lower panel). We found a subset of POA^{Trpm2} neurons (21%) with correlated activity upon T_{core} increase (24/116, n = 5 mice). Given that the change in T_{POA} is tightly correlated with changes in T_{core} (Figure 1C), these neurons likely represent WSNs responding to a local POA temperature increase. Nevertheless, again we found no enrichment of these presumed WSNs in the POA^{Trpm2} population.

In summary, these data show that POA^{Trpm2} neurons are neither exclusively found nor enriched within the population(s) of WSNs and WRNs, suggesting that expression of TRPM2 is not demarcating either population and raising the possibility that the ion channel may promote hypothalamic temperature sensing outside these two neuronal subgroups.

Temperature sensitivity of WSNs is enhanced by TRPM2 ion channel activity

Given that *Trpm2* expression does not constitute a “genetic marker” for the WSN population, we wondered whether TRPM2 had any impact on WSN function. Indeed, we found a significant reduction in temperature sensitivity of *Trpm2*$^{-/-}$ WSNs as evidenced by a reduced TC, producing a reduced firing rate increase for a given warmth stimulus (Figures 4I and S5A). We only observed this effect in WSNs as AP firing patterns of moderately warm-sensitive neurons (MSNs; 0.2 Hz/°C < $TC_{(MSN)}$ < 0.8 Hz/°C) and warm-insensitive neurons (ISNs; –0.6 Hz/°C < $TC_{(ISN)}$ < 0.2 Hz/°C) were not altered in the absence of TRPM2 (Figures 4I and S5A), suggesting that the ion channel specifically modulates WSNs. The influence of TRPM2 on WSN temperature sensitivity was further confirmed pharmacologically: the TRPM2 inhibitor 2-Aminoethoxydiphenyl borate (2-APB) (Togashi et al., 2008) also reduced warmth sensitivity in WSNs (Figure S5B). 2-APB is not specific for TRPM2 (Hu et al., 2004; Xu et al., 2005). However, the drug did not further reduce temperature sensitivity in WSNs from *Trpm2*$^{-/-}$ slices but rather had the opposite effect

(Figure S5C), which could be the result of compensatory expression (or unmasking) of other thermosensitive ion channels activatable by 2-APB (Hu et al., 2004) in mice lacking TRPM2. These results demonstrate that TRPM2 specifically enhances temperature sensitivity of WSNs.

TRPM2 modulates synaptic drive to WSNs to enhance preoptic temperature sensitivity

Because TRPM2-gating in response to warming would result in membrane depolarization, we speculated that WSNs might display altered baseline membrane potentials in the absence of TRPM2. However, baseline potentials determined in preoptic WSNs of *Trpm2*$^{-/-}$ and control mice were similar at 36°C (mean ± SD: –58 ± 6 mV [n = 37] and –55 ± 6 mV [n = 34], respectively; p = 0.06; Dunn's test) and at 39°C (–53 ± 6 mV [n = 37] and –51 ± 8 mV [n = 34]; p = 0.8; Dunn's test). Also, the TRPM2 inhibitor 2-APB had no discernible effect on baseline potentials of wild-type and *Trpm2*$^{-/-}$ WSNs (36°C: mean ± SD; *Trpm2*$^{+/+}$: –53 ± 4 mV [n = 19]; *Trpm2*$^{-/-}$: 54 ± 4 mV [n = 11]; p = 0.69, Dunn's test; 39°C: mean ± SD; *Trpm2*$^{+/+}$: –50 ± 4 mV [n = 19]; *Trpm2*$^{-/-}$: –51 ± 4 mV [n = 11]; p = 0.54; Dunn's test). Additionally, the resting membrane potential of WSNs measured in the presence of tetrodotoxin (TT×) to block ongoing AP firing revealed no differences at 36°C (*Trpm*$^{+/+}$: –52 ± 6 mV [n = 9]; *Trpm2*$^{-/-}$: –53 ± 9 mV [n = 8]; p = 0.9; Student's t test).

It has been suggested that faster depolarization in between APs (the so-called depolarizing prepotential) may increase firing rates in WSNs exposed to warmer temperatures (Griffin et al., 1996). Averaging the depolarization rate of the prepotential in WSNs did not reveal any differences between *Trpm2*$^{-/-}$ and control WSNs (Figure S5D). More generally, analyzing the average AP waveforms of *Trpm2*$^{-/-}$ and wildtype WSNs at different temperatures also did not point to any gross alterations that could explain differences in their temperature sensitivity (Figure S5E). In conclusion, TRPM2 appears not to directly mediate temperature-dependent depolarization of WSNs.

Moreover, when exposing the cytosolic side of WSNs to ADP-ribose, an intracellular-acting TRPM2 agonist (Perraud et al., 2001; Sano et al., 2001), we did not observe any agonist-evoked currents (Figures S5F and S5G; n = 6 for POA^{Trpm2} WSNs and n = 5 for randomly sampled WSNs), corroborating that TRPM2 does not affect intrinsic properties of WSNs to shape their activity.

Albeit surprising, all our data are congruent with a thermosensitive function of TRPM2 outside of WSNs. In consequence, we considered a role of TRPM2 in modulating synaptic inputs to WSNs. To probe this possibility, we utilized synaptic blockers (CNQX [10 μM], AP5 [50 μM], Gabazine [20 μM]) in our POA brain slice experiments (Figure S5H).

Unexpectedly, synaptic blockade was sufficient to void the effect of *Trpm2* deletion: temperature-induced firing of *Trpm2*$^{-/-}$ WSNs in the presence of synaptic blockers increased significantly (Figure 4J). Activity of ISNs was also slightly altered in the presence of synaptic blockers, but this effect was similar (albeit not identical) in POA neurons of wild-type and *Trpm2*$^{-/-}$ mice (Figures S5I and S5J), demonstrating that TRPM2 primarily modulates synaptic inputs to WSNs, which markedly influences their temperature-sensitive AP firing (Figures 4I and S5A).

Preoptic warm sensitivity is governed by synaptic activity

Thermosensitivity of WSNs has been attributed to cell-autonomous firing-rate changes, largely independent of synaptic input and orchestrated by somatically expressed ion channels (Boulant, 2006; Kobayashi et al., 2006). However, it is possible that a more prominent role of synaptic drive in preoptic thermosensitivity has escaped attention.

To monitor WSNs in an unbiased fashion over long stimulation periods, we implemented SomArchon-based voltage imaging (Piatkevich et al., 2019) to record AP spiking of POA neurons in brain slices (Figure 5A). The voltage sensor allowed robust spike detection over long periods of time and applying several consecutive temperature ramps (Figures 5B, S6A, and S6B). Most importantly, we were able to identify WSNs similarly to classic electrophysiological recordings (Figure 5C). Notably, we observed a larger number of bursty neurons in our voltage-imaging recordings that were not as prominently represented in electrophysiological recordings (Figures S6C-S6E), potentially explaining (at least partially) the slightly smaller fraction of WSNs in voltage-imaging experiments (11%).

In agreement with previous studies (Hori et al., 1980; Kelso and Boulant, 1982), we found that synaptic blockade does not abolish warm sensitivity per se. But, surprisingly, when recording neuron activity sequentially before and after synaptic blocker application, we found that all but one WSN became warm-*in*sensitive while a few previously ISNs or cold-sensitive neurons (CSNs) instead became warm sensitive (Figures 5D-5F). Firing rates of both WSNs and CSNs were particularly amenable to synaptic modulation, in comparison to the bulk of ISNs that did not change firing (Figures 5D, S6F, and S6G).

Probing the synaptic contribution to WSN activity electrophysiologically, by sequentially washing in glutamatergic, as well as glutamatergic and GABAergic, synaptic transmission blockers, demonstrated that extensive local excitatory, inhibitory, and disinhibitory inputs modulate WSN firing frequency (Figures 5G-5J). Collectively, these findings demonstrate an unrecognized and prominent role of synaptic activity in determining warm sensitivity of POA neurons.

TRPM2 enhances presynaptic calcium influx at warm temperatures and increases neurotransmitter release

Given that synaptic input strongly modulates warm sensitivity of preoptic neurons, we wondered whether the calcium-permeable TRPM2 channel may act as a temperature sensor in presynaptic terminals. We specifically directed a calcium sensor to fiber terminals by adeno-associated virus (AAV) delivery of a synapto-physin-GCaMP6s fusion protein into the POA of wild-type and *Trpm2*$^{-/-}$ mice (Figures 6A-6C and S7A). Preparing acute brain slices of these animals allowed us to detect calcium transients of randomly selected preoptic fiber terminals before and after a temperature increase from 33°C to 37°C. The detected calcium transients likely arose from both stochastic opening of presynaptic calcium-permeable ion channels such as TRPM2 and APs reaching the presynapse. We found that a warming stimulus increased the frequency and duration of the calcium transients in a subpopulation of presynaptic terminals (Figure 6D), while calcium transients remained unchanged or decreased in other terminals. When computing the area under the

curve (AUC) of the $\Delta F/F_0$ traces recorded at 33°C and 37°C (allowing quantification of the total calcium inflow per fixed time interval) and plotting the distribution of the integrated calcium response magnitude ($AUC3_{37°C}/AUC_{33°C}$) for all fiber terminals in a histogram, we found that overall—and despite the response heterogeneity—warming-induced calcium increases were significantly reduced in *Trpm2*$^{-/-}$ fiber terminals (Figure 6E).

These results suggest that TRPM2 may localize to presynaptic boutons where it can increase synaptic transmitter release dynamics upon warming by permitting presynaptic calcium entry. To test this hypothesis directly, and to assess whether TRPM2 has the ability to act as a synaptic temperature sensor, we recorded miniature excitatory and inhibitory postsynaptic currents (mEPSCs and mIPSCs, respectively) at two different temperatures by randomly patching POA neurons in brain slices prepared from wild-type and *Trpm2*$^{-/-}$ mice. When shifting the temperature from 29°C to 36°C, we found a general increase in the frequency of postsynaptic events. This is consistent with the reported temperature dependence of the presynaptic transmitter release machinery (Sabatini and Regehr, 1996). Strikingly, TRPM2 robustly and significantly enhanced the frequency of mIPSCs, but not mEPSCs, upon warming (Figures 6F-6H). On the other hand, the amplitude of miniature synaptic currents was not significantly altered, neither for excitatory nor inhibitory postsynaptic responses (Figures S7B and S7C), arguing against a potential role of presynaptic TRPM2 in regulating quantal size. Altogether, our results support a presynaptically restricted, thermosensory role of TRPM2 in inhibitory POA synapses.

Next, we assessed whether expressing TRPM2 presynaptically would be sufficient to generate a thermally active synapse that enhances neurotransmission at high temperatures. To this end, we differentiated induced pluripotent stem cells (iPSCs) into synaptically connected neurons *in vitro* (Zhang et al., 2013). Little to no endogenous TRPM2 protein is found in these cultured neurons, allowing us to precisely control expression of TRPM2 in the pre- or postsynaptic neuron by viral delivery (Figures S8A, S8B, and S9A). We found that the frequency of miniature postsynaptic currents increased in a temperature-sensitive way only when TRPM2 was virally expressed in the presynapse but not in the postsynapse (Figures S8C and S8D). In agreement with recordings in native POA brain slices (Figures 6F-6H, S7B, and S7C), this finding further corroborated a presynaptic thermosensory mechanism for TRPM2. Likewise, the amplitude of synaptic currents was not significantly altered. Instead, we found the rise time of miniature events to be accelerated (Figures S8C and S8D), suggesting that synaptic vesicle fusion pores opened faster when TRPM2 was thermally activated presynaptically (Guzman et al., 2010). Thus, warming-induced calcium influx via TRPM2 into the presynapse likely enhances the rate and speed of synaptic vesicle fusion in presynaptic terminals. Consistently, we found overexpressed TRPM2 protein to be localized not only in the somatic compartment of induced neurons but also in fiber terminals (Figures S9A and S9B). Of note, TRPM2-mediated synaptic modulation in the derived model neurons was already measurable at 36°C, while perisomatic calcium responses were detected only at >40°C (Figure S9C).

In summary, the data obtained from the iPSC-derived model synapse recapitulated results obtained in native POA slice preparations of wild-type and *Trpm2*$^{-/-}$ mice and demonstrate

that TRPM2 can function as a presynaptic temperature sensor, operating in the physiological temperature range.

POA^{Trpm2} neurons can mediate local synaptic disinhibition

Because *in situ* hybridization and the Trpm2-Cre reporter mouse line indicated Trpm2 expression in neurons residing within the POA (Song et al., 2016; Zhang et al., 2020), we considered a local POA network of TRPM2-containing synapses that could mediate body cooling upon local POA warming (Figures 3A, S2E, and S2F). To assess whether POA^{Trpm2} neurons are locally connected to neighboring POA neurons, we employed an optogenetic approach and virally expressed Cre-dependent channelrhodopsin (AAV-ChR2) in the POA of Trpm2-Cre mice. Brain slice recordings permitted us to activate POA^{Trpm2} neurons by light stimulation while simultaneously recording AP firing activity of neighboring neurons (Figures S10A and S10B). We found a total of 62% neurons to be functionally connected to local POA^{Trpm2} neurons, with the majority being inhibited (53% of all neurons, which amounts to 85% of all functionally connected neurons; Figure S10B), in line with the observation that Trpm2 expression is predominantly detected in inhibitory POA neurons (Song et al., 2016).

We considered different local POA connectivity scenarios that could possibly explain the effect POA^{Trpm2} neurons have on the thermosensitivity of WSNs. Because WSNs exhibit reduced temperature-dependent AP firing rates and TC in the absence of TRPM2 (Figures 4I and 4J), and the channel appeared to exclusively promote inhibitory neurotransmission (Figures 6G and 6H), we considered a disinhibitory circuit motif (Wang and Yang, 2018) to mediate warming-induced POA^{Trpm2}→WSN activation. A disinhibitory model predicts that activation of inhibitory POA^{Trpm2} neurons would activate—disinhibit—WSNs via an intermediate inhibitory neuron (Figure 7A). To assess whether a local preoptic disinhibitory circuit motif, arising from inhibitory POA^{Trpm2} ($POA^{Trpm2/Vgat}$) neurons, exists, we virally expressed channelrhodopsin (AAV-ChR2) in a Cre- and FlpO-recombinase-dependent fashion in the POA of Trpm2-Cre;Vgat-FlpO mice (Jo et al., 2018) (Figure 7A).

As expected, some recorded neurons (25%) reduced firing rates when optically activating $POA^{Trpm2/Vgat}$ cells, likely reflecting direct inhibition. Intriguingly, another group was instead activated upon optic stimulation of inhibitory $POA^{Trpm2/Vgat}$ neurons (Figure 7B), a fraction (11%) similar in size to that of WSNs (Figure S6C). Application of excitatory transmission blockers had no effect on light-stimulated activation, while abrogating inhibitory transmission blocked light-induced activity (Figure S10C), suggesting that local preoptic disinhibition can be triggered by inhibitory POA^{Trpm2} neurons (Figure 7A).

Next, we asked whether WSNs are connected to POA^{Trpm2} neurons using *ex vivo* optogenetic stimulation. Indeed, we found that identified WSNs can increase their firing when neighboring POA^{Trpm2} neurons were optically activated (Figure 7C). We found that POA^{Trpm2} neurons also modulate select ISNs and CSNs (Figure S10D), confirming the voltage-imaging experiments (Figure 5D) and demonstrating extensive local POA connectivity arising from POA^{Trpm2} neurons.

Collectively, our data highlight a synaptic mechanism of preoptic warm sensitivity and thermoregulation, with TRPM2 as one synaptic component that can modulate WSN activity upon temperature increase to drive body cooling (see graphical abstract).

Discussion

A large body of literature has characterized POA WSNs, hypothesizing that their most salient feature—an increase in AP firing upon warming—is a cell-autonomous, pacemaker-like property (Boulant, 2006; Madden and Morrison, 2019; Tan and Knight, 2018).

A role for TRP channels in POA temperature sensing has previously been proposed. One study described a heat-induced, TRP channel-like depolarizing current in cultured preoptic neurons that, in principle, could mediate temperature-sensitive AP firing (Kobayashi et al., 2006). Using similarly dispersed cultures of neonatal mice absent of any synaptic connections, we previously found a TRPM2-dependent, heat-induced depolarizing calcium current (Song et al., 2016). At the time, we presumed these cells to be WSNs, not knowing then that warm sensitivity is a network feature shaped by synaptic input. Here, using acute POA brain slice preparations to keep local synaptic architecture intact, we did not find any evidence for a warming-induced depolarizing current that drives WSN AP firing, in agreement with previous brain slice studies (Boulant, 2006).

Possibly, severing neuronal connections and culturing of POA neurons may have affected TRPM2 redistribution to perisomatic cell membranes, thereby giving rise to prominent somatic responses *in vitro.* It is also plausible that immature neurons used in previous culturing experiments express TRPM2 more broadly, in both synaptic and extra-synaptic compartments.

Interestingly, recent reports demonstrate different thermal thresholds observed for TRPM2 in cultured sensory neurons (>45° C) in comparison to behavioral thermosensation and thermoregulation (33°C-40°C) (Mulier et al., 2020; Ota et al., 2019; Song et al., 2016; Tan and McNaughton, 2016; Vandewauw et al., 2018; Vilar et al., 2020). Here, our iPSC-derived model neuron experiments suggest higher and lower TRPM2-dependent activation thresholds at the cell soma (>40°C; Figure S9C) and synapse (~36°C; Figure S8C), respectively. Possibly, different temperature sensitivities of perisomatic versus synaptic TRPM2 — or different sensitivities of calcium measurements versus synaptic current recordings—may account for this discrepancy. Alternatively, an intriguing possibility is that the kinetics of the temperature stimulus may explain the different responses, with fast heat stimuli producing robust somatic (high-threshold) responses, while slower/steady-state (low-threshold) temperature changes rather modulate (longer-lasting) TRPM2-dependent presynaptic calcium currents. Future biophysical studies will be required to shed light on the underlying mechanistic differences.

On the mRNA level, *Trpm2* appears to be expressed in both inhibitory and excitatory neurons, with a preponderance in inhibitory neurons (Song et al., 2016). While a temperature-induced, TRPM2-mediated boost of excitatory input onto WSNs would be the most parsimonious synaptic configuration explaining the increase of WSN activity

upon warming, our data rather suggest that TRPM2 increases inhibitory synaptic output to stimulate—or rather "gate"—WSN activity by disinhibition (Figures 6G and 6H). In our local POA connectivity analysis, however, we found both local disinhibition and direct synaptic excitation to modulate preoptic WSNs (Figures 5G-5J). Thus, local disinhibition appears to be the predominant $POA^{Trpm2}\rightarrow$WSN circuit motif, but direct excitation cannot be excluded. Future studies probing recently defined excitatory and inhibitory preoptic cell populations (Moffitt et al., 2018) may help to elucidate local preoptic circuit configurations that mediate thermoregulation.

It is possible that synaptic temperature detection contributes to other temperature sensitive, neuro-thermoregulatory pathways besides the hypothalamus, such as the spinal cord and solitary tract nucleus (NTS) (Jessen, 1985; Peters et al., 2010). Several temperature-sensitive TRP channels are transported to central sensory afferent fiber terminals innervating the spinal cord and NTS, suggesting the possibility that deep body temperature changes may be detected at spinal and supra-spinal pre-synaptic terminals to modulate transmitter release.

Our results show that deletion of the *Trpm2* gene does not abolish warm sensitivity of WSNs but that the channel thermally influences synaptic outputs that modulate WSN activity. In this regard, it is important to note that our new data are not in disaccord with decades-old findings that cell-intrinsic (somatic) warm sensitivity modulates AP firing rates in preoptic neurons. It rather suggests that temperature-sensitive synaptic input from the POA local network may, in a way, "keep tabs" on intrinsic (temperature-sensitive) activity of POA neurons and thus provide an additional level of thermoregulatory control.

What could be the overarching role of thermally active synapses in controlling WSN function and thermoregulation? The thermoregulatory center requires weighing various variables to generate finely tuned outputs that maintain temperature homeostasis in a context-dependent manner. As such, circadian, metabolic, inflammatory (fever), and other variables influence T_{core} regulation. Disinhibitory circuit motifs are ideally suited to regulate pathway gating and have, for example, been implicated in routing information flow in the hippocampus and cortex (Möhler and Rudolph, 2017).

We observed that thermode-driven, warming-induced, long-lasting hypothermia was dependent on TRPM2 (Figures S2E and S2F), which could be explained by the ion channel's capacity to mediate thermally induced synaptic plasticity. Thus, adaptive changes to long-lasting thermal challenges may be another function of synaptic temperature detection and integration.

At the extreme end, our results, in particular those derived from voltage-imaging experiments employing synaptic blockers, may suggest that synaptic inputs define thermoregulatory cell categories and that the classic cell-intrinsic categorization of WSNs, MSNs, ISNs, and CSNs is obsolete. However, for two reasons, we believe such conclusions are currently too premature and not (yet) justified. First, pharmacological-induced synaptic blockade is an extreme scenario that *in vivo* very likely never occurs. Second, our findings using $Trpm2^{-/-}$ mice also argue in favor of (at least partially) stable thermoregulatory cell categories: deleting the *Trpm2* gene or pharmacologically blocking its function alters the

firing rate and TC of WSNs (but not that of ISNs or CSNs; Figures 4I and S5A-S5C) and reduces the body-cooling response upon thermode stimulation *in vivo* (Figures 3A, S2E, and S2F). This, for the first time, suggests a physiological link between WSN activity and thermoregulation (body cooling) and argues that the definition of a WSN may still be relevant and useful—at least to some extent.

According to classic models of POA thermosensitivity, neuronal coding of temperature information (and, thus, thermoregulatory outputs) has been presumed to be linearly correlated to an increase in AP firing rates in WSNs, culminating in a thermo-centric definition of neuronal categories based on the TC (Boulant and Dean, 1986). While this model is attractive, it likely is an oversimplification. Our voltage-imaging experiments revealed additional activity patterns that may carry temperature information across the POA network. Next to linear AP firing rate increases, we also observed modulation of AP burst patterns by warming (Figures S6C and S6D), casting a new light on the definition of WSNs. Future *in vivo* (somatic, synaptic, and network) activity measurements in combination with computational approaches may reveal a more complete picture of temperature information processing for thermal homeostasis.

Star*Methods

Key Resources Table

Reagent Or Resource	Source	Identifier
Antibodies		
Sheep polyclonal anti-DIG-AP	Roche	RRID: AB_514497
Chicken polyclonal anti-MAP	BioLegend	RRID: AB_2564858
Rabbit polyclonal ant-synapsin1,2	Synaptic Systems	RRID: AB_887804
Rat monoclonal anti-TRPM2	This paper	N/A
Rabbit polyclonal anti-Na-K-ATPase	Cell Signaling Technology	RRID: AB_2060983
Rabbit monoclonal anti-NeuN	Abcam	RRID: AB_2889250
Bacterial and virus strains		
AAV5.EFa.Flex.taCasp3.TEVp	Addgene	45580-AAV5
AAV5.EF1a.DIO.Synaptophysin-GCaMP6s	Addgene	105715-AAV5
AAV-1/2-hSyn1-dlox-hM3D(Gq) _mCherry(rev)-dlox-WPRE-hGHp(A)	Viral Vector Facility from the University of Zurich	v89-1
AAV1 .Syn.Flex.GCaMP6s.WPRE.SV40	University of Pennsylvania Gene Therapy Program Vector Core	AV-1-PV2821
AAV1/2.ShortCAG.dlox.SomArchon_EGFP(rev).dlox.WPRE.SV40	Viral Vector Facility from the University of Zurich	v462-1
AAV1/2.hSyn1.chl.iCre.WPRE.SV40	Viral Vector Facility from the University of Zurich	v223-2

Reagent Or Resource	Source	Identifier
AAV-DJ/2-hSyn1-chI-dlox-hChR2(H134R)_mCherry(rev)-dlox-WPRE-hGHp(A)	Viral Vector Facility from the University of Zurich	v332-DJ
Lentivirus TetO-EGFP	Produced in the lab	N/A
Lentivirus hUbC-TRPM2	Produced in the lab	N/A
Lentivirus TetO-EGFP	Produced in the lab	N/A
Chemicals, peptides, and recombinant proteins		
PGE_2	Sigma	P6532
4QH-tamoxifen	Sigma	H7904
Sunflower seed oil	Sigma	55007
Castor oil	Sigma	239853
CNQ	Enzo	BML-NS105-0025
ADP Ribose	Sigma-Aldrich	A0752
2-APB	Abcam	ab120124
SR 95531 hydrobromide (Gabazine)	Hello Bio	HB0901
D-AP5	Hello Bio	HB0225
Tetrodotoxin citrate	Hello Bio	HB1035
CNQX disodium salt	Hello Bio	HB0205
Experimental models: Cell lines		
iPSC	DKFZ/ University Hospital Mannheim	HD6
Experimental models: Organisms/strains		
Trpm2$^{-/-}$ mouse: B6;Trpm2$^{tm1Yamo/}$Uhg	Yasuo Mori	MGI:3803341
Trpm2^{Cre} mouse:Trpm2$^{tm1.1(icre)Jsmn}$	Interfacultary Biomedical Faculty, University of Heidelberg	RRID: IMSR_JA×:029647
Trpv1^{cre} mouse: B6.129-Trpv1$^{tm1(cre)Bbm}$/J	The Jackson Laboratory	RRID: IMSR_JA×:017769
Trpm3$^{-/-}$ mouse: Trpm3^{tm1Lex}	Lexicon Genetics	MGI:3528836
Rosa-DTA mouse : Gt*(ROSA)26*$^{Sortm1(DTA)Jpmb}$/J	The Jackson Laboratory	RRID: IMSR JAX:006331
FosTRAP2 mouse: B6.129(Cg)-Fos$^{tm1.1(cre/ERT2)Luo}$/J	The Jackson Laboratory	RRID: IMSR JAX:021882
TdTomato mouse: Gt(rosa)26Sor$^{tm9(CAG-tdTomato)Hze}$/J	The Jackson Laboratory	RRID: IMSR JAX:007909
LepR$^{-/-}$ mouse: *B6.BKS(D)-Lepr*^{db}/J	The Jackson Laboratory	RRID: IMSR_JAX:000697
Recombinant DNA		
Full-length RNA probe anti-mouse TRPV1	Produced in the lab	N/A
Full-length RNA probe anti-mouse TRPM8	Produced in the lab	N/A

Europe PMC Funders Author Manuscripts

Reagent Or Resource	Source	Identifier
Plasmid pMD2.G	Addgene	12259
Plasmid pRSV-rev	Addgene	12253
Plasmid pMDLg/pRRE	Addgene	12251
Plasmid FUW-M2rtTA	Addgene	20342
Plasmid FUW-TRPM2	This paper	N/A
Plasmid pTet-O-Ngn2-puromycin	Addgene	52047
Software and algorithms		
MATLAB for Windows version R2016a-2020a	MathWorks	N/A
GraphPad Prism for Windows V5.00 and V7.00	GraphPad software	N/A
R version for Linux 3.6.1	R Consortium	N/A
Igor Pro 6.11 - 6.37	WaveMetrics	N/A
Metafluor Software	Molecular Devices	N/A
MetaMorph 7.1 Software	Molecular Devices	N/A
ImageJ/Fij	ImageJ Consortium	N/A
Thermes USB Data Acquisition	Physitemp	N/A
Ponemah Physiology Platform V6.41.20418.1 software	DSI	N/A
MicroManager1.4 software package	Vale's lab, UCSF, USA	N/A
SPOT advanced	SPOT imaging, Michigan, USA	N/A
Clampex 11.0.3, pClamp 10.3	Molecular Devices, USA	N/A
Patchmaster 2.30, Patchmaster 10	HEKA, Lambrecht, Germany	N/A

Resource Availability

Lead contact

Further information and requests for resources and reagents should be directed to and will be fulfilled by the lead contact Jan Siemens (jan.siemens@pharma.uni-heidelberg.de).

Materials availability

The TRPM2 antibody and plasmids generated to virally overexpress TRPM2 generated in this study will be made available on request, but we may require a payment and/or a completed Materials Transfer Agreement if there is potential for commercial application. This study did not generate any other unique reagents.

Experimental Model And Subject Details

All animal care and experimental procedures were approved by the local council (Regierungspräsidium Karlsruhe, Germany) under protocol numbers 35-9185.81/

G-150/13,35-9185.81/G-168/15, G-201/16 and 35-9185.81/G-169/18. Mice were housed under standard conditions with a 12 h light/dark cycle and *ad libitum* access to food and water. All genetically-modified mice in this study were on the C57BL/6N background. Most studies employed a mixture of male and female mice, unless specified. The animals were randomly assigned for experiments and the experimenter was aware of the animal genotype when conducting experiments. Mice between 6 weeks and 5 month of age were used in the experiments. Number of animals per experimental group and gender are detailed in Table S1.

Method Details

Brain cannula implantation (thermometer/thermode holder)

All surgical procedures were performed under aseptic conditions and deep anesthesia. Before surgery, animals were anesthetized using an intraperitoneal (i.p) injection of Medetomidin 0.5 mg/kg, Midazolam 5 mg/kg and Fentanyl 0.05 mg/kg. Fur of the head was removed, skin disinfected (Braunol; Braun, Germany) and cornea moisture was preserved during surgery by the application of eye ointment (Bepanthen; Bayer, Germany). Mice were placed on a stereotaxic apparatus (Model 1900; Kopf, USA) under a custom made (INF workshop) heating pad set at 37°C. A craniotomy of approximately 1 mm diameter was drilled with a hand drill (QS40; Osada Electric, Japan). A 5 mm length before pedestal stainless steel guide cannula (0.90 mm QD and 0.58 mm ID; model C311GS5/SPC; Plastic One, USA) was implanted unilaterally in the POA (coordinates from Bregma: ML:0.500 mm, AP: 0.800) and secured using dental cement (Paladur; Heraeus, Germany). Right after implantation, a dummy cannula of 5 mm in length was screwed onto the guide cannula to prevent dust from entering the brain (model C311DCS5/SPC; Plastic One, USA). Skin was sutured with sterile absorbable-needled sutures (Marlin 17241041; Catgut, Germany). After the surgery, the anesthesia was antagonized using a subcutaneous injection of Antipamezol 2.5 mg/kg, Flumazenil 0.5 mg/kg and Naloxon 1.2 mg/kg and mice were transferred to their home cages. For postoperative care, mice were injected subcutaneously with Carprofen at 5 mg/Kg (Rimadyl; Zoetis, USA), kept on a heating pad at 37°C for 12 h and monitored closely to verify full anesthesia recovery. Animals were allowed to fully recover from the surgery for at least one week before any further procedure. Mice implanted with brain cannulas were housed individually.

Telemetry transmitter implantation

The surgical procedure was performed under aseptic conditions and deep anesthesia. Animals were anesthetized using an i.p injection of Medetomidin 0.5 mg/kg, Midazolam 5 mg/kg and Fentanyl 0.05 mg/kg. Fur of the abdomen was removed, skin disinfected (Braunol; Braun, Germany) and cornea protected with eye ointment (Bepanthen; Bayer, Germany). A sterile telemetric transmitter (TA11TA-F10; Data Sciences International, USA) was implanted in the abdominal cavity. Thereafter, muscle and skin layers were separately sutured with absorbable surgical threads (Marlin 17241041; Catgut, Germany). After the surgery, the anesthesia was antagonized using a subcutaneous injection of Antipamezol 2.5 mg/kg, Flumazenil 0.5 mg/kg and Naloxon 1.2 mg/kg. For postoperative care, mice were injected subcutaneously with Carprofen at 5 mg/kg (Rimadyl; Zoetis, USA), kept on a

heating pad at 37°C for 12 h in their home cage and monitored closely to verify anesthesia recovery. Animals were allowed to fully recover from the surgery for at least one week before any further procedures.

POA temperature measurement

Our POA thermometers/thermodes were made in-house using an ultra-thin thermocouple (0.13 mm wire diameter and 0.23 mm sensor tip diameter; IT-24P; Physitemp, USA) adhered with thermo-conductive silicon glue (SE4486; Corning, USA) to a 6 mm length tutor and mounting threat (C315DS/SPC; Plastic One, USA). The thermocouple wire in contact with brain tissue was further protected with a medical-grade polyimide tube (ID 0.31 mm, QD 0.34 mm; Microlumen, USA). The external wire of the thermocouple was secured with Tygon tubing and glued externally to the tutor using non-toxic silicone (Kwik-Cast; World Precision Instruments, USA). During the experiments, the POA thermocouple was fixed to the head of the animals using the thread of a guide cannula. Once connected to the head of a mouse, approximately 0.5 to 1 mm (depending on skull bone thickness) of the thermocouple (containing the sensor tip, the only temperature-sensitive part of the thermocouple) would stick out of the tube of the 5 mm long guide cannula and enter the POA.

CTX and POA temperature measurement device

The overall design of our double CTX and POA thermometers was similar to the POA temperature measurement device described above. Particularly, a second ultra-thin thermocouple (IT-24P; Physitemp, USA) was fixed approximately 4 mm from the POA sensor tip. Once connected to the head of a mouse using a 1 mm long guide cannula, the CXT thermocouple would stick out of the tube of guide cannula approximately at the level of the motor CTX and the POA thermocouple would be placed in the center of the POA.

Circadian CTX, POA, and body temperature measurements

Animals were connected to the two brain thermometers/thermodes using the thread of the previously implanted guide cannula. Mice connected to the brain thermometer were housed individually and allowed to move freely with *ad libitum* access to food and water. Radio signals encoding core body temperature were sampled by receiver plates under the home cages (RSC-1, DSI, USA) using Ponemah Physiology Platform V6.41.20418.1 software (DSI, USA) while brain temperatures were acquired at 1 Hz by Thermes USB Data Acquisition and DasyLab V12.00.00 software (Physitemp, USA). The implantation sites were verified *postmortem* by tracking the scar left by the guide cannula on the tissue.

PGE_2 microinjection and simultaneous POA and body temperature measurements

On the day of the experiment, mice were connected to the POA thermometer/thermode and handled as described before. Using an automatic microinjector (UMP3 with SYS-micro4 controller; WPI, USA), 2 μL of a solution containing 2 nmol/μl PGE_2 (P6532; Sigma, USA) in DMSQ:NaCl 0.9% endotoxin-free 1:1 was injected into the POA at 1 μl/min through an injection cannula of 6 mm length (C315I/Spc; Plastic One, USA). After brain injection, mice were returned to the home cage and the POA and body temperature measurements

continued. Data was further collected for at least 2 more h. The implantation sites were verified as mentioned above.

Short-term heat stress and simultaneous POA and body temperature measurements

To perform quick changes in ambient temperature, we used a custom-made thermic chamber. Radio signals encoding core body temperature were sampled by receiver plates under the thermic chamber (RSC-1, DSI, USA) using Ponemah software (DSI, USA) while brain temperatures were acquired at 1 Hz by Thermes USB Data Acquisition (Physitemp, USA). Mice were monitored for 1 h before heat stress. During heat stress, the chamber temperature was risen from baseline (30°C) to 38°C for 15 min and then quickly returned to baseline. Recording continued for 20 min after heat stress.

Thermode design

Qurbrain thermode was modeled after a previously published model used in birds (Long and Fee, 2008). Briefly, a silver wire (99.99%) of 200 μm in diameter (AG-8W; Science Products, Germany) was soldered to the hot plate of a thermoelectric cooler (TEC) (00701-9B30-22RU4; Custom Thermoelectric, USA) and used as thermode. To protect the TEC from overheating and improve performance, a heat sink of 1 cm^3 was made of 145-wires-per-inch copper mesh (200x200C0020W40T; TWI inc, USA) and soldered to the cold plate of the TEC. The whole length of thermode (with the exception of the last 1 mm) was insulated with a medical-grade polyimide tube (ID 0.41 mm, QD 0.44 mm; Microlumen, USA). A thin sheet of air between the silver wire and the polyimide tube worked as a second layer of thermal insulation between the thermode and surrounding tissue. A layer of styrofoam of 2 mm (Styrofoam HD300 330/480 2mm; Styrocut, Germany) was placed between the TEC and the mounting threat (C315DS/SPC; Plastic One, USA) for further insulation. The mounting threat was then glued to the thermode externally using non-toxic silicone (Kwik-Cast; World Precision Instruments, USA). On the experimental day, the thermode was secured to the head of the animals using the thread of a guide cannula implanted at least two weeks before thermode stimulation. Once connected to the head of a mouse, approximately 0.5 to 1 mm (depending on skull bone thickness) of the uninsulated tip of the thermode would stick out of the 5 mm long guide cannula and enter the POA for thermal stimulation.

In vitro estimation of stimulation temperatures

During *in vivo* experiments, the thermode temperatures were measured using an ultra-thin thermocouple (0.13 mm wire diameter; IT-24P; Physitemp, USA) fixed below polyimide tube with thermo-conductive silicon glue(SE4486; Corning, USA) at 1 mm from the tip of the thermode. To estimate the temperature at the tip of the thermode during experiments, a second thermocouple was fixed at the tip of the thermode. Then, the thermode was placed in a chamber at 37°C (the heat sink was at room temperature, mimicking the *in vivo* conditions). A ramp of voltages (0.2, 0.4 and 0.6 mV) was applied to the TEC and the temperatures at tip of the thermode and 1 mm from tip were simultaneously measured. The steady state temperatures per condition were estimated by fitting the measured temperatures to an exponential function (Long and Fee, 2008). A linear function between the steady state temperatures at tip and 1 mm from tip was estimated from these *in vitro* experiments. This

linear function was then used to estimate the real stimulation temperature at the tip of the thermode during the *in vivo* experiments.

In vivo thermode performance measurements

To evaluate the performance of the thermode stimulation *in vivo,* mice were implanted bilaterally with two brain guide cannulas (C311GS5/SPC; Plastic One, USA) as described before. On the day of the experiment, mice were connected simultaneously to the thermode and contralaterally to a brain thermometer/thermode and were housed individually with *ad libitum* access to food and water. A ramp of voltages (0.5 and 0.7 mA) was applied to the TEC and the temperatures at the thermode and contralateral to the thermode were registered. The steady state temperatures per condition were estimated as described before. The distance between the tip of the thermode and the brain thermometer was verified *postmortem* using micro CT scanning.

Thermode stimulation and body temperature measurements

On the day of the experiment, animals were connected to the thermode using the thread of the previously implanted guide cannula. Thereafter, mice were housed individually with *ad libitum* access to food and water and were allowed to recover from handling stress at least two h before performing POA warming experiments. Radio signals encoding core body temperature were sampled by receiver plates under the home cages (RSC-1, DSI, USA) using Ponemah (DSI, USA) while thermode stimulation temperatures were acquired at 1 Hz by Thermes USB Data Acquisition (Physitemp, USA). A power supply (HMP2030; Rohde&Schwarz, Germany) was used to control the current through the TEC. The stimulation sites were verified *postmortem* by tracking the scar left by the guide cannula and thermode on the tissue.

Thermode stimulation in $Trpv1^{Abl}$ and $Trpv1^{WT}$ mice

Hemizygous$Trpv1^{Cre}$ mice were crossed with hemizygous Rosa-DTA animals to produce experimental mice as described in (Mishra et al., 2011). $Trpv1^{Abl}$ mice carried $Trpv1^{Cre}$ and Rosa-DTA alleles while $Trpv1^{WT}$ animals were only positive for either $Trpv1^{Cre}$ or Rosa-DTA alleles. Adults $Trpv1^{Abl}$ and $Trpv1^{WT}$ animals (2 to 4 months) were implanted with brain cannulas and telemetric transmitter (TA11TA-F10; Data Sciences International, USA) as described before.

Stereotactic viral injection and thermode stimulation in $Trpm2^{Abl}$ mice

Stereotactic injections were performed as previously described (Song et al., 2016). All surgical procedures were performed under aseptic conditions and deep anesthesia. Adult $Trpm2^{Cre(+)}$ mice were anesthetized using an i.p. injection of Medetomidin 0.5 mg/kg, Midazolam 5 mg/kg and Fentanyl 0.05 mg/kg. Fur of the head was removed, skin disinfected and cornea moistened as described earlier. Mice were placed on a stereotaxic apparatus (Model 1900; Kopf, USA) and kept warm using a heating pad at 37°C. Two craniotomies of approximately 0.25 mm diameter were drilled at each side of the skull with a hand drill (OS40; Osada Electric, Japan). A pulled-glass capillary with 20-40 μm tip diameter was lowered into the brain and virus was injected using an air pressure system

at two positions (1: Bregma: ML: 0.400 mm, AP: 0.800 mm, DV: −4.750 mm; 2: ML: −0.4.000 mm, AP: 0.800 mm and DV: −4.750 mm). 250 nL recombinant adeno-associated virus (rAAV) encoding the Cre-dependent caspase 3 gene (Yang et al., 2013) (AAV5.EF1a. Flex.taCasp3.TEVp; Addgene Core; USA) was injected at each coordinate. Finally, the anesthesia was antagonized using a subcutaneous injection of Antipamezol 2.5 mg/kg, Flumazenil 0.5 mg/kg and Naloxon 1.2 mg/kg and mice were transferred to their home cages. Postoperative care was performed as described before. Subsequent brain cannula and telemetry implantation and thermode stimulation were performed in Trpm2$^{Cre(+)}$ mice as explained in previous sections.

Stereotactic viral injection and thermode stimulation in FosTRAP2 mice

Stereotactic surgeries were performed in adult FosTRAP2 mice as described in previous sections. For these experiments, 250 nL of rAAV encoding the Cre-dependent excitatory Gq-DREADDs (AAV1/2.hSyn1.dlox.hM3D(Gq)_mCherry(rev).dlox.WPRE.hGhp(A); Viral Vector Facility from the University of Zurich; Switzerland) was injected bilaterally at Bregma: ML: ± 0.400 mm, AP: 0.800 mm, DV: −4.750 mm. After virus injection, a brain cannula was implanted unilaterally as described earlier. Finally, the anesthesia was antagonized and mice were transferred to their home cages. Postoperative care was performed as described before. Subsequent telemetry implantation and thermode stimulation were performed in FosTRAP mice as detailed in previous sections. Directly before the beginning of the thermode stimulation period, control as well as thermode-stimulated mice received a single i.p. injection of 50 mg/kg of 4OH-tamoxifen (H7904; Sigma) diluted in 4:1 sunflower seed oil (55007; Sigma): castor oil (239853; Sigma). After trapping, Gq-DREADD expression was allowed to proceed for 2 weeks. Reactivation of TRAPped cells was performed by injecting CNO 0.3 mg/kg i.p. (Enzo, diluted in saline) while body temperature was monitored as mentioned above.

Stereotactic viral injection in Trpm2^{Cre} mice and vGat-FlpO;Trpm2^{Cre} mice

Stereotactic surgeries were performed in adult Trpm2^{Cre} and in vGat-FlpO;Trpm2^{Cre} mice as described in previous sections. For these experiments, animals were injected bilaterally with 250 nL of rAAV(DJ) encoding the Cre-dependent ChR2, at Bregma: ML: ± 0.400 mm, AP: 0.800 mm, DV: -4.750 mm. In order to further distinguish ChR^{+} from ChR2^{-} neurons, in the Trpm2$^{Cre(+)}$ line, rAAV(DJ) encoding the Cre-dependent ChR2 was also injected at the same Bregma point. Finally, the anesthesia was antagonized and mice were transferred to their home cages. Postoperative care was performed as described above.

Stereotactic viral injection and lens implantation

Stereotactic injections were performed as described before. Specifically, a craniotomy of approximately 1 mm diameter was drilled in adult Trpm2^{Cre} mice. 250 nL of a dilution 1:3 to 1:5 in sterile saline of rAAV encoding the Cre-dependent calcium indicator GCaMP6s (Chen et al., 2013) under control of the human synapsin-1 promoter (AAV1.Syn.Flex.GCaMP6s.WPRE.SV40, University of Pennsylvania Gene Therapy Program Vector Core, USA) was injected two positions (1: Bregma: ML: 1.000 mm, AP: 0.700 mm, DV: −5.080 mm, head angle 10°; 2: ML: 1.000 mm, AP: 0.900 mm and DV: −5.080 mm, head angle 10°). After virus injection, a gradient refractive index lens was

slowly implanted (133 μm/min) (Bregma: ML: 1.000 mm, AP: 0.800 mm and DV: −4.750 mm, head angle 10°) using a motorized arm (Mini 25 Linear Actuator; Luigs&Neuman, Germany). The lens was secured to the cranium using dental cement (Paladur; Heraeus, Germany). The surface of the lens was then covered with non-toxic silicon glue (Kwik-Cast; World Precision Instruments, USA). After the implantation, the skin was sutured with sterile absorbable-needled sutures (Marlin 17241041; Catgut, Germany). The anesthesia was antagonized using a subcutaneous injection of Antipamezol 2.5 mg/kg, Flumazenil 0.5 mg/kg and Naloxon 1.2 mg/kg and mice were transferred to their home cages. Postoperative care was performed as described before. 4 weeks after virus injection and under deep anesthesia, the silicon cover of the lens was removed, the surface of the lens was cleaned using acetone and a metal baseplate was secured onto the head of the mouse. The implantation sites were verified *postmortem* by tracking the scar left by the lens on the tissue and the expression of GCaMP6s.

Data acquisition, extraction of calcium traces, and identification of temperature responding neurons

GCaMP6s signals were acquired using in-house made miniature fluorescent wide-field microscopes (UCLA Miniscopes) (Ghosh et al., 2011). Miniscopes were manufactured following descriptions available at http://miniscope.org. On the day of the experiment, animals were connected to the miniscope and transferred to our thermic chamber with *ad libitum* access to food and water. After 2 h of habituation, ambient temperature was changed. The neural calcium activity in freely-moving animals was recorded using the data acquisition software developed within the Miniscope Project (freely available under http://miniscope.org). Motion correction and calcium trace extraction were performed by a custom built pipeline written in MATLAB that combined multiple available open source repositories (indicated below). Briefly, .avi files obtained from the Miniscope software were first memory mapped. A rigid motion correction algorithm was then used to correct the raw data (Cai et al., 2016). The spatial footprints of ROIs and neuropil corrected calcium traces were extracted automatically using a constraint non-negative matrix factorization approach optimized for microendoscopic imaging data (namely CNMF-E) followed by manual curation (Zhou et al., 2018). ROIs with abnormal spatial features (e.g., ROIs detected on the edges of the lens) were discarded. Z-scores of the extracted calcium signals from each imaging session were clustered into two groups (potentially, responders and not responders) using k-means (k = 2). The Pearson correlation coefficient between each calcium trace (z-score) and its corresponding ambient or body temperature trace was calculated. A randomized (re)sample of these correlation coefficients was generated using a bootstrapping approach in which each calcium trace was circle-shifted a random number of frames (keeping overall activity unchanged) and the correlation coefficient between the randomized calcium traces and the corresponding temperature trace was calculated. We repeated this process 10,000 times for each dataset (imaging session) to generate a randomized distribution of correlation coefficients. We defined the upper and lower 5% quantiles of these randomized distributions (similar to a p value of 0.05) as a statistical criterion to categorize the recorded calcium traces as significantly correlated (positively or negatively) to temperature (responder cells).

POA slice preparation for electrophysiology

5 to 14 week old *Trpm2*$^{+/+}$ or *Trpm2*$^{-/-}$ mice were deeply anaesthetized using isoflurane. Upon acute decapitation, the head was immediately submersed in ice-cold carbogenated slicing solution (in mM): 85 NaCl, 2.5 KCl, 10 Glucose, 75 Sucrose, 1.25 NaH_2PO_4, 25 $NaHCO_3$, 3 $MgCl_2$, 0.1 $CaCl_2$, 3 MyoInositol, 2 NaPyruvate, 0.4 Ascorbic Acid and the brain was acutely dissected. 300 μm thick coronal brain slices were made in ice-cold oxygenated slicing solution using a vibratome (Leica VT1200). Slices were transferred and incubated for 30-60 min at 37°C in a carbogenated incubation solution (in mM): 109 NaCl, 4 KCl, 35 Glucose, 1.25 NaH_2PO_4, 25 $NaHCO_3$,1.3 $MgCl_2$,1.5 $CaCl_2$. After this incubation slices were kept at room temperature (RT) until placed in the recording chamber.

Electrophysiological recordings in acute brain slices

Cell attached or whole-cell recordings were established using an EPC10 amplifier controlled by Patchmaster 2.30 software (HEKA; Lambrecht, Germany) and the cells were visualized by dodt gradient contrast (Luigs-Neumann, Germany), using an Olympus (BX51 WI) upright microscope equipped with a water immersion objective (20×, UMPlanFL N, Olympus; 60×, LUMIFI, Olympus, Japan). Images were digitally acquired using a Spot monochromatic real time infrared sensitive camera (Visitron Systems GmbH, Germany), using the Spot Advanced software (SPOT Imaging, Michigan, USA). Data was sampled at 20 kHz and filtered using Bessel linear filters. In voltage-clamp mode, data was filtered by a 3 pole 10 kHz Bessel filter (filter 1) in series with a 4 pole 2 kHz Bessel filter (filter 2) and subject to series resistance compensation (100 μs). In current-clamp mode, data was filtered using a 2.9 kHz4-pole Bessel filter. All data was analyzed using custom scripts written in MATLAB (MathWorks) or Prism 6 software (GraphPad).

All recordings were performed in a modified carbogenated artificial cerebrospinal fluid solution (aCSF, in mM) 125 Na Cl, 6.25 KCl, 30-33 Glucose (for osmolarity adjustment), 1.25 NaH_2PO_4, 25 $NaHCO_3$, 1.3 $MgCl_2$, 2.4 $CaCl_2$. ~320 mOsm/L (Zhao and Boulant, 2005). Using an agar bridge saturated with 3 M KCl between the chamber and the ground electrode, to keep the ground electrode at RT and isolate it from the temperature changes applied to the chamber (Zhao and Boulant, 2005). For general synaptic blockade, 50 μM D-AP5,10 μM CNQX and 20 μM Gabazine were added to aCSF. For membrane potential (V_m) measurements, 1 μM TTX was added to aCSF. For TRPM2 blockade 100 μM 2-APB was added to aCSF. Glass micropipettes (1.5 mm QD, WPI, 1B150F4) were pulled using a Flaming/Brown micropipette puller (model P-97; Sutter Instruments Co., USA).

For whole-cell current-clamp (I-Clamp) recordings, pipettes with 2 MU to 6 MΩ open tip resistance in aCSF were used, filled with low chloride intracellular solution containing (in mM): 138 K Gluconate, 2 KCl, 5 NaCl, 10 HEPES, 10 EGTA, 1 $CaCl_2$,1 Mg-ATP. (295 ± 5 mOsm., pH = 7.2 adjusted with KOH), with a liquid junction potential of 12 mV in aCSF (corrected in the reported recordings). For whole-cell voltage-clamp (V-Clamp) recordings of sIPSCs, pipettes were filled with high chloride intracellular solution, containing (in mM): 115 CsCl, 10TEA-Cl, 25 HEPES, 3 Mg-ATP, 0.5 Na-GTP, 0.5 EGTA, (300 ± 5 mOsm., pH = 7.2 adjusted with CsOH), with a liquid junction potential of −8 mV in aCSF (corrected from the recordings reported). The holding potential (V_h) was −85 mV. To determine which

cell category was being recorded, AP firing rate changes in response to temperature were recorded in cell-attached configuration (high Cl^- intra) in V-Clamp mode, adjusting V_h to maintain a 0 nA leak current. After cell-attached recordings, break in was produced and V-Clamp recordings were performed at 36°C. During long term V-clamp recordings, series resistance was continuously monitored and adjustments in compensation were performed as needed.

To evaluate ADPR-evoked TRPM2 currents, IV curves were recorded as described before. Briefly, a 500 ms descending voltage ramp from +40 mV to -120 mV was applied in V-Clamp mode, with a 500 ms prepulse at +40 mV to inactivate voltage gated conductances and a 500 ms posterior step at -120 mV. To determine which cell category was being recorded before intracellular ADPR infusion, AP firing rate changes in response to temperature were recorded in cell-attached configuration as described above. After cell-attached recordings, break in was produced and IV curves were recorded in V-Clamp mode < 20 s from break in, 2.5 or 5 min after, at 33-36°C.

All recordings were performed at 33°C to 39°C, by running carbogenated aCSF at 2 mL/min in a perfusion system including an inline heater and a chamber solution temperature probe (heat control system and digital thermometer, MPI, Heidelberg) mounted on a temperature-controlled microscope stage (Luigs & Neumann, Badcontroller V). Chamber solution temperature was constantly monitored. A ~6 min. sinusoid temperature stimulus was applied through the in line heater stepping between 36°C baseline, 39°C, 33°C and back to 36°C baseline; or alternatively 36°C baseline, 33°C, 39°C and back to 36°C baseline. The order of the stimulation steps (33°C - 39°C or 39°C - 33°C) did not seem to affect cell categorization. Chamber temperature sometimes drifted to temperatures lower than 33°C and higher than 39°C, nevertheless chamber temperature never surpassed 42°C. The temperature-controlled microscope stage was set to a constant temperature of 33°C which buffered abrupt temperature changes in the chamber during stimulation.

Electrophysiological recordings and optogenetic stimulation in acute brain slices

Acute brain slices from 5 to 14 week old *Trpm2*$^{+/+}$ or *Trpm2*$^{-/-}$ and Trpm2$^{Cre(+)}$ mice or vGat-FlpO;Trpm2$^{Cre(+)}$ mice were prepared in the manner and with solutions described before. AP firing changes in response to temperature were recorded in the whole-cell current-clamp mode by using MultiClamp 700B amplifier (Molecular Devices, USA), sampled at 10 kHz, filtered using Bessel linear filters and digitized with the Axon Digidata 1550B (Molecular Devices, USA) using Clampex 11.0.3 software (Molecular Devices, USA). Cells were visualized by SliceScope (Scientifica, UK) upright microscope, with water immersion objective (40X, Olympus U-TV1X-2, Olympus, Japan) by phase contrast light imaging. Image was acquired by digital CCD camera (ORCA-R2 C10600-10B, Hammatsu Photonics K.K., Japan) using MicroManager1.4 software package (Vale's lab, UCSF, USA).

Recordings were performed at the sinusoid temperature ramp of 33°C, 36°C and 39°C, by running carbogenated aCSF (described before) through the bath at the flow of 2 mL/min, with a gravity-driven ValveLink 8.2-system (AutoMate Scientific, USA). In order to maintain stable bath temperature and achieve sinusoid stimulus with 3 temperatures, temperature controller (CL-100, Warner Instruments, USA) was connected to a thermistor

probe placed at bath chamber (V4.1 PCT Mini Chamber, Luigs and Neumann, Germany), controlled by temperature controller (Temperaturcontroller VII, Luigs and Neumann, Germany) and liquid cooling device (LCS-1 Heat Exchanger KOOLANCE, Warner Instruments, US).

Synaptic blockers, D-AP5, CNQX disodium salt, and Gabazine (SR95531 hydrobromide) (HelloBio, UK), were used in the same concentration as described before. Grounding electrode was protected from temperature changes in the bath by 3M KCl agar bridge. Borosilicate glass micropipettes used (O.D. 1.5 mm, I.D. 0.86 mm, Sutter Instrument, BF150-86-7.5) were pulled on a micropipette puller (P-97, Sutter Instrument, USA). The open pipette resistance measured was between 4-10 MU. Recording pipettes were filled with the low chloride intracellular solution described in previous sections. To illuminate neurons infected with channelrhodopsin within the POA, blue light (470 nm) pulses were supplied by a light-emitting diode (LED)-based optical system (pE-100 CoolLed, Scientifica, UK). The target site was illuminated with 10-ms light pulses at 5 Hz. Each train of the light pulses was given for 20 s.

Where both optogenetic stimulation and warm sensitivity were recorded, light stimulation was applied first to confirm the connectivity of the neuron following by the temperature ramp. Synaptic blockers were applied and the optogenetic stimulation was repeated in the presence of either D-AP5 and CNQX or all three blockers. Where possible, the temperature ramp was repeated in the presence of the synaptic blockers in order to examine the possible switch in temperature sensitivity described by voltage imagining. Analysis was done by customized MATLAB R2020a (MathWorks, USA) and Igor Pro 6.37 (WaveMetrics, USA) scripts in addition to GraphPad Prism 7 software (GraphPad, USA).

Derivation and electrophysiological recording of induced human neurons (referred to as “iGluts”)

First, for selective *‘presynaptic expression of TRPM2’,* three groups of iPSCs were generated. Group #1 was infected with a cocktail of lentiviruses expressing *Ngn2,* full-length rat *Trpm2,* and tdTomato. Group #2 was infected with lentiviruses expressing *Ngn2* and tdTomato. Group #3 was infected with lentiviruses expressing *Ngn2* and nuclear *Gfp* (nGFP). Four days later, cells were detached and re-seeded on Matrigel-coated coverslips in the following permutations/ratios: for the *experimental condition,* cells from group #1 and group #3 were mixed-up at a ratio of 80/20%, respectively. For the control condition, cells from group #2 and group #3 were mixed-up at a ratio of 80/20%, respectively. All recordings were performed from GFP+/TdTomato-cells. This experimental configuration allowed testing the impact of selective presynaptic expression of TRPM2 on synaptic transmission.

Second, for selective ‘postsynaptic expression of TRPM2’ a similar approach was used, but with some modifications. Group #1 was infected with lentiviruses expressing *Ngn2*, full-length rat *Trpm2,* and nGFP. Group #2 was infected with lentiviruses expressing *Ngn2* and tdTomato. Group #3 was infected with lentiviruses expressing *Ngn2* and nuclear *Gfp* (nGFP). Four days later, cells were mixed-up in the following permutations/ratios: for the *experimental condition,* cells from group #1 and group #2 were mixed-up at a ratio

of 20/80%, respectively. For the control condition, cells from group #2 and group #3 weremixed-upat a ratio of 80/20%, respectively. All recordings were performed from GFP+/TdTomato-cells. This experimental configuration allowed to test the impact of selective postsynaptic expression of TRPM2 on synaptic transmission.

All electrophysiological measurements were performed 4-5 weeks after derivation, in the presence of 0.5 μM TTX in the external solution. On the day of recordings, coverslips containing iGluts prepared as described above were placed in a recording chamber mounted onto an Olympus BX51WI upright microscope equipped with DIC and fluorescence capabilities. Recordings were performed at 33°C or 36°C. Chamber temperature was controlled using a TC-344C, dual (in line +chamber temperature) temperature control system (Warner). Batch temperature in recording chamber, was also independently monitored using Physitemp temperature probe. Cells were approached and patched under DIC with 3 MegaOhm pipettes pulled from borosilicate glass (Warner instruments, Inc) using a vertical Narishige PC-10 puller (Japan). Neurons were maintained at −70 mV holding potentials using a HEKA EPC10 amplifier (HEKA; Lambrecht, Germany) controlled by Patchmaster 10 software (HEKA; Lambrecht, Germany). Series resistance in all experiments varied between 8-10 MegaOhms. Recordings in which series resistance was higher than that were not included in the analysis. iGluts in the recording chamber were continuously perfused with oxygenated (95% O2/5%CO2) bath solution containing (in mM): 125 NaCl, 2.5 KCl, 1 MgCl2, 2 CaCl2, 25 glucose, 1.25 NaH2PO4, 0.4 ascorbic acid, 3 *myo*-inositol, 2 Na-pyruvate, and 25 NaHCO3 pH 7.4., and 315 mOsm. Miniature currents were recorded with an internal solution that contained (in mM): 140 Cs-Methanesulfonate, 0.5 EGTA, 1 MgCl2,10 HEPES, 2 ATP-Magnesium, 0.4 GTP-Sodium, 10 Na-PhosphoCreatine, pH 7.2,310 mOsmoles. Detection and analysis of miniature currents properties was performed offline using custom-written macros in IgorPro 6.11 (Wavemetrics).

Electrophysiological recording of mEPSC and mIPSCs in mouse brain slice preparations

Acute brain slices were prepared as described above. Miniature postsynaptic current measurements of POA neurons in acute brain slices prepared from *Trpm2*$^{+/+}$ and *Trpm2*$^{-/-}$ mice were recorded similar to those described for induced human neurons (iGluts) above, but using a slightly different internal solution (in mM): 140 Cs-Gluconate, 0.2 EGTA, 5 MgCl2, 40 HEPES (pH 7.3 with CsOH), 2 Mg-ATP and 0.3 Li-GTP, 315 mOsmoles. 0.5 μM TT× was always present in the external solution to record spontaneous currents only. mEPSC were recorded at -60 mV and mIPSCs at 9 mV holding potentials (liquid junction potential: -9 mV). Miniature postsynaptic currents were recorder over a time period of 100 s (10 sweeps of 10 s each) and detected and analyzed using Clampfit (Molecular devices), using a typical mIPSC/mEPSC waveform obtained after averaging mIPSC or mEPSC events, respectively. mIPSC/mEPSC properties were plotted in Prism and IgorPro.

Voltage imaging in acute brain slices

C57BL/6N and *Trpm2*$^{-/-}$ animals between 5 to 7 weeks of age were injected unilaterally in the POA as described before. Briefly, a sparse labeling of preoptic neurons with the cre-dependent genetically encoded voltage indicator SomArchon

(Piatkevich et al., 2019) was achieved by injecting 200 nL of a mixture 1:1 of undiluted rAAV encoding SomArchon (AAV1/2.ShortCAG.dlox.SomArchon_EGFP(rev). dlox.WPRE.SV40) mixed together with 1:1000 diluted rAAV coding for the recombinase iCre(AAV1/2.hSyn1.chl.iCre.WPRE.SV40). Both viral preparations were obtained from the Viral Vector Facility of the University of Zurich. Thereafter, infections proceeded for two weeks before using animals for experiments.

On the day of the experiment, acute mouse brain slices were prepared as described before (Song et al., 2016). Mice were deeply anesthetized using an intraperitoneal injection of ketamine (Ketavet; Zoetis, USA) and xylazine (Rompun; Bayer, Germany), decapitated and brains dissected out. 250 μm thickness POA sections were prepared using a vibration microtome (HM 650 V; Themo Scientific, USA) filled with carbogen-bubbled NMDG-HEPES solution at 4°C containing (mM): NMDG 93, KCl 2.5, NaH2PO4 1.2, L(+) ascorbic acid 5, Thiourea 2, sodium pyruvate 3, $MgSO_4.7H_2O$ 10, $CaCl_2.2H_2O$ 0.5, HEPES 20, $NaHCO_3$ 30, Glucose 25 and N-acetyl-L-cysteine 10, titrated to pH 7.3 with HCl 37%[65]. After slicing, POA containing coronal slices were recovered for 15 min in carbogen-bubbled NMDG-HEPES solution at 32°C and thereafter were transferred to a holding chamber containing carbogen-bubbled aCSF(mM): NaCl 125, KCl, 2.5, $NaHCO_3$ 25, NaH_2PO_4 1.25, $MgCL_2$ 1, $CaCL_2$ 2 and glucose 25 (Ting et al., 2014)

Voltage imaging was performed using an upright microscope (BX51W; Olympus, Japan) coupled to a motorized base plate (SliceScope SS-1000-00; Scientifica, UK), a 40X objective (LumPlanFL N; Olympus, Japan) and a sCMOS camera (Zyla 4.2; Andor Technology, UK). A 470 nm excitation illumination (pE-2; cooledLED, UK) and a standard GFP filter set were used to visualize GFP and identified SomArchon-expressing neurons. SomArchon imaging was achieved using a 637 nm laser (OBIS LX 100mW; Coherent; USA), a ZT640rdc dichroic mirror and an ET655lp emission filter (both from Chroma Technology; USA). Voltage imaging frequency acquisition was set at 1 kHz in a cropped camera chip and using binning 8.

All recordings were performed in a modified carbogenated artificial cerebrospinal fluid solution as described before, gassed with 95% O_2 and 5% CO_2 at 3 mL/min. General synaptic blockade was achieved as mentioned above. Bath temperature was monitored using a thermistor (TA-29, Warner Instrument, USA). Changes in bath temperature were performed with an in-line temperature controller (CL-200; Warner Instruments, USA) commanded externally using an A/D board (Digidata 1440A, Molecular Devices, USA) and pClamp 10.3 software (Molecular Devices, USA). Each imaging session lasted for 20 s and was performed once bath temperature was stabilized at the desired set points (typically between 33-34°C, 35-36°C and 37-38°C).

Images were acquired using MetaMorph 7.1 (Molecular devices, USA). The fluorescence time course of each neuron was measured by averaging all pixels within the regions of interest (ROIs) using ImageJ. Baseline correction and calculation of z-scores were performed using custom scripts written in R version for Linux 3.6.1 (https://www.r-project.org). When required, a high pass filter (Butterworth filter with a cut frequency of 0.04) was used. Subsequently, spike detection was performed following a threshold and

maximum method as described before (Piatkevich et al., 2019). Briefly, data points where z-score were > 3 SD over the whole recording were identified. Within these data points, spikes were identified as the maximum value within 3 consecutive pictures.

Presynaptic calcium-imaging in acute brain slices

Sparse labeling of POA neurons (pAAV-Ef1a-DIO-Synaptophysin-GCaMP6s, Addgene: #105715-AAV5) acute slice preparation, imaging and temperature stimulation were performed following the voltage imaging procedures described earlier. The microscope was calibrated to determine the exact pixel size (0.43x0.43 microns) and frames of 682x682 px were collected at 5Hz in full chip and binning 3. Raw image sequences were corrected for photobleaching and background signal by subtracting to each frame a Gaussian blur of itself (sigma = 20). Motion artifacts brought by the temperature stimulation were corrected using template matching rigid motion correction. ROI segmentation was automatically performed through thresholding the standard deviation projections of background, bleaching and motion corrected image sequences. Threshold was set to 2 times the average gray value of the whole frame. Only ROIs of 0.86-2.15 microns in diameter were analyzed to make sure the extracted signal came from presynaptic terminals.

Extracted calcium traces were corrected for temperature dependent changes in baseline fluorescence using the ratio of the average fluorescence at 33°C over 37°C as a correction factor for the fluorescence recorded at 37°C. ΔF/F0 was calculated using the 10% quantile of the overall fluorescent signal, corrected for temperature, as F0. ΔF/F0 traces were normalized to the overall maximum and the area under the curve of the normalized ΔF/F0 traces was calculated using a trapezoidal approximation.

In situ hybridization

In situ hybridizations were performed as previously described (Song et al., 2016). Briefly, mice were killed in accordance with ethical guidelines of the local governing body and brains, DRGs and TGs were freshly dissected, embedded into OCT and frozen on dry ice. 20 µm cryo-sections were cut (CM3050S; Leica, Germany), collected on Super-Frost Plus slides (Fisher Scientific, USA) and stored at -80°C until use. Tissue from ablated animals ($Trpv1^{Abl}$) was collected, side by side, on the same slide together with tissue from control animals ($Trpv1^{WT}$) for better expression comparisons. *In situ* hybridization was performed using standard protocols (Watakabe et al., 2007). DIG-labeled cRNA probes were hybridized overnight at 65°C. Sections were washed at 60°C in 2xSSC/50% Form-amide/ 0.1% N-lauroylsarcosine with 20 µg/mL RNase A for 15 min at 37°C. Next, tissue was washed twice in 2xSSC/0.1% N-laur-oylsarcosine at 37°C for 20 min and twice in 0.2xSSC/ 0.1% N-lauroylsarcosine at 37°C for 20 min. Sections were blocked in MABT/10% serum/1% blocking reagent (11096176001; Roche, Switzerland). Sections were incubated overnight with sheep anti-DIG-AP (1:1000; 11093274910; Roche, Switzerland). Staining was performed using NBT/BCIP in NTMT until satisfactory intensity. *Trpm8* and *trpv1* probes covered the ORF of the respective genes.

β-Galactosidase staining

Trpm3$^{-/+}$ animals were killed in accordance with ethical guidelines of the local governing body and transcardially perfused with PBS followed by 4% PFA. Brains were dissected out and cryo-protected with 30% sucrose in 1X PBS at 4°C. 20 μm cryo-sections were cut (CM3050S; Leica, Germany), collected on Super-Frost Plus slides (Fisher Scientific, USA) and stored at -80°C until use. For the staining, sections were air-dried at RT for 1 h and washed three times in rinse buffer (100 mM sodium phosphate pH 7.3,2 mM MgCl, 0.01% sodium deoxycholate, 0.02% NP-40). β-Galactosidase staining was performed at 37°C in a solution containing 5 mM potassium ferrocyanide, 5 mM potassium ferricyanide and 1 mg/mLX-gal in rinse buffer. Thereafter, slides were washed three times in 1 × PBS and sections were mounted on glass slides in Immu-Mount (Fischer Scientific, USA).

αTRPM2 antibody production and TRPM2 immunochemistry

To determine if TRPM2 can be expressed in somatic and axonal compartments in induced neurons (iGluts), we specifically labeled the somatodendritic (postsynaptic) or axonal (presynaptic) compartments with specific antibodies, in combination with TRPM2 immunostaining. Specifically, iGluts with or without TRPM2 expression were harvested 4-5 weeks after differentiation, washed with PBS at 37°C twice, and then fixed with 4% paraformaldehyde at room temperature for 20 min. Once fixed, the samples were permeabilized with 0.2%triton x-100, blocked with 5% normal goat serum, and incubated overnight at 4°C with primary antibodies against MAP (Chicken, 1:1000, BioLegend San Diego, USA) and TRPM2 (rat, 1:100, custom produced) and synapsin1,2 (rabbit, 1:500, custom produced) to assess co-localization in somato-dendritic compartments. Next day, iGluts were washed in PBS (3-times) and incubated for 2 h with secondary (1:1000) antibodies conjugated to different Alexa dyes as follows: Alexa 586 anti-rabbit and Alexa 643 anti-rat antibodies for MAP/TRPM2 or Synapsin/TRPM2 combinations. All Alexa-conjugated antibodies were purchased from Jackson ImmunoResearch. Synaptic structures were imaged using a confocal microscope (Leica, Germany) controlled by LAS X software (Leica, Germany). Specimens were sampled in frame mode at 1024*1024 pixels/frame resolution. 10 optical sections along the z axis were taken for each sample and then compiled into a single maximal projection image for analysis. All the acquisition parameters were kept constant between conditions and experiments.

Immunocytochemistry to detect the synaptic calcium indicator Synapto-GCaMP6s

Mice expressing AAV-synapto-GCaMP6s virus were killed in accordance with ethical guidelines of the local governing body and transcardially perfused with PBS followed by 4% PFA. Brains were dissected out, kept in sucrose gradient (10% followed by 30% until completely sank). Brains were sectioned with a microtome at 30 μm thickness and sections were kept in cryo-protectant solution at 4°C until the free-floating staining was performed. For the staining, sections were washed 1 time in PBS and left overnight at 4°C in 0.2% Triton X-100 (PBX0.2). On the following day, sections were blocked with 5% goat serum in PBS containing 0.1% Triton X-100 (PBX0.1) for 2 h at room temperature (RT). Sections were then incubated with chicken aGFP (1:500; Novus Biologicals, NB100-1614) and mouse α-SV2A (1:250; DSHB Hybridoma Product SV2), diluted in 1% goat serum

in PBX0.1) for 3 days at 4°C. On the fifth day, sections were washed extensively with PBX0.2 and then incubated with secondary antibodies and DAPI (Alexa488 α-chicken 1:750, Alexa555 α-mouse 1:750) for 4 h at RT. Finally, tissue was washed extensively with PBSX0.2 and 1 time with PBS after which it was mounted using Immu-Mount (FisherScientific, UK).

Histological and cytological image acquisition and analysis

Bright field images were taken on Nikon Eclipse Ts2 and a Ni-E wide field microscope (Nikon imaging center, Heidelberg). Confocal images were acquired with a Nikon C2 Plus microscope (Nikon imaging center, Heidelberg). Images were processed and analyzed using ImageJ/Fiji, Adobe Photoshop and Illustrator. Contrast and brightness were adjusted for visualization purposes only but without altering the information content of the images. Brain schemes were modified from Paxinos and Franklin, 2001.

Temperature sensitivity behavioral test

Temperature sensitivity was tested using a Hot/Cold Plate Assay (Bioseb, Vitrolles, France).

Western blot

C57BL/6N, $Trpm2^{Cre(+)}$ and $Trpm2^{Cre(-)}$ animals were killed in accordance with ethical guidelines of the local governing body and brains were dissected out. By using a brain matrix, a 1 mm thick coronal section encompassing the medial POA was cut out. The slice was further trimmed to mostly dissect the POA. For western analysis, either the whole tissue was lysed or membrane fractions were prepared. For the latter, the tissue was homogenized in 300 µl cold homogenization buffer using a glass-teflon dounce homogenizer. To gather the maximum amount of tissue lysate, the douncer was rinsed with an additional 500 µl of homogenization buffer. The homogenate was centrifuged at 4°C, at 1000xg for 10 min. The supernatant was ultracentrifuged at 100.000xg for 1 h at 4°C using a TLA 110 rotor to separate the plasma membrane fraction from the cytosolic fraction. The pellet was resuspended in 50ul cold RIPA buffer containing protease inhibitors (complete, Roche) and PSMF (100uM) and used for western blot. For some western blots, the POA tissue was homogenized in a douncer in 300ul RIPA buffer containing protease inhibitors and PMSF, centrifuged at 1000xg for 10min at 4°C and the supernatant used for analysis without further fractionating.

In the case of human iPSC-derived iGlut neurons, lysates were taken from two 24 wells using 100ul cold RIPA buffer containing protease inhibitors and PMSF. The lysates were centrifuged at 14000rpm for 5 min at 4°C and the supernatant used for western blot analysis.

Protein lysates were loaded on 3%-8% polyacrylamide gels and proteins were separated at 150V in 1x NuPage Tris-Acetate SDS running buffer using the Xcell SureLockTM mini cell system (Invitrogen). The gel was incubated in 0.02% SDS in 2x transfer buffer for 10min and then blotted onto a polyvinylidene fluoride (PVDF) membrane using the 1xNuPage transfer buffer for 1 h at 30V. The membrane was blocked in 5% BSA in tris-buffered saline containing Tween (TBST) for 1 h at RT and then cut into two pieces between the marker bands indicating 120 and 85kDa. The upper part was incubated in a custom made

rat anti TRPM2 antibody (1:500) and the lower part in a rabbit Na-K-ATPase antibody (Cell Signaling Technology, 1:3000) or in the case of iGlut neurons, in a mouse Synapsin 1 antibody (Synaptic Systems, 1:4000) in 1% BSA at 4°C overnight. The membrane was washed three times in TBST and incubated in goat anti-rat HRP (Life Technologies, 1:5000), goat anti rabbit HRP (Jackson/Dianova,1:5000) or goat anti mouse HRP (Jackson/Dianova, 1:3000) respectively, in 1% BSA in TBST for 2 h at RT. Protein bands were developed using the enhanced chemiluminescence (ECL) Prime Western Blotting Detection Reagent from Amersham. The membrane signals were detected using an ImageQuant LAS 4000 system.

The western blot bands were analyzed using ImageJ. For this purpose the region of interest (the bands for TRPM2 as well as Na^+/K^+ATPase) was determined using the rectangle tool. The pixel intensities for TRPM2 were divided by those for the respective Na^+/K^+ATPase to normalize each band. The average value for the three control bands was calculated and divided by the value for each sample ($Trpm2^{Cre(+)}$). The average and standard deviation of the samples was calculated and expressed in percent with the average of the control band being 100%.

Calcium imaging in iPSC-derived model neurons

Glass coverslips containing iPSC-derived model neurons (iGLUTs), infected with lentiviral constructs expressing jGCaMP7 with/without lentivirus expressing TRPM2, were placed in a diamond shaped chamber (Warner Instruments, USA) constantly perfused (~4 mL/min) with Ringer's solution ((mM): 140 NaCl, 5 KCl, 2 CaCl2, 2 MgCl2, 10 HEPES and 10 glucose, adjusted with NaOH, to pH 7.4) containing TTX (500 nM Tetrodotoxin citrate, Hello Bio, UK). Solution was run by a gravity-driven perfusion system (Valve-BankII, AutoMate Scientific, USA). Calcium-imaging was performed using an inverted fluorescent microscope (Axio Observer. D1, Carl Zeiss, Germany) equipped with a 10X objective (Fluar 10X/0.5 M27, Carl Zeiss, Germany) and a sCMOS camera (Zyla4.2, Andor Technology, Oxford Instruments, UK).

To test the temperature response of iGLUTs, 3 temperature stimuli (approximately 37°C, 40°C, 45°C) of 45 s duration were applied to the cells, with 3 min room temperature intervals between each stimulus. Temperature stimuli were generated using an in-house made glass coil system connected to a water bath (MultiTemp III; Pharmacia Biotech, Sweden) pumping the waterto the coils. Temperature at the chamber was measured by thermocouple probe (IT-18; Physitemp Instruments, USA) placed immediately next to the coverslip. The chamber temperature was simultaneously recorded along with the calcium signals. Cells were excited at the wavelength of 480 nm (GFP filter set), images were obtained with 4Hz acquisition rate in Metafluor Software (Molecular Devices, USA).

As a last stimulus, cells were perfused with high K^+ Ringer solution [(mM): 45 NaCl, 100 KCl, 2 $CaCl_2$, 2 $MgCl_2$,10 HEPES and 10 glucose, adjusted with NaOH to pH 7.4] to visualize typical neuronal response to potassium.

Motion correction on videos, cell registration and signal traces extraction were performed using Suite2p pipeline (Pachitariu M., Stringer C., Howard Hughes Medical Institute

Janelia Research Campus, code accessible under https://github.com/cortex-lab/Suite2P) and analyzed with R packages. The cut-off to consider a cell a responder was set as the mean response of all imaged cells during the application of the temperature stimulus (TRPM2(+) as well as TRPM2(-)) plus one SD.

Quantification And Statistical Analysis

Data was analyzed using R version for Linux 3.6.1 (https://www.r-project.org), RStudio for Linux version 1.1.463 and MATLAB for Windows version R2016a-2020a (MathWorks, USA). Statistical tests were performed using GraphPad Prism for Windows V5.00-7.00 (GraphPad software, USA). Results are presented as mean ± standard error of the mean (SEM) unless indicated otherwise. Distribution of data was assayed using the KS normality test, the D'agostino and Pearson omnibus normality test and the Shapiro-Wilk normality test. Further statistical details are listed in table S1. Star, '*', signifies $p < 0.05$, '**' $p < 0.01$, and '***' $p < 0.001$.

Supplementary Material

Refer to Web version on PubMed Central for supplementary material.

Acknowledgments

We thank Yasuo Mori for *Trpm2*$^{-/-}$ mice and Annika von Seggern and Daniela Pimonov for technical support; members of the Siemens lab for inspiring discussions and critical input; Rebecca Mease and Henning Fenselau for valuable criticism and reading of the manuscript; Ed Boyden, Zeguan Wang, and Demian Park for help with setting up voltage-imaging; Jorg Pohle for support with electrophysiological recordingsand Manfred Jugold for assistance with microCT measurements; and the Nikon Imaging Center at Heidelberg University for support with confocal microscopy. The authors gratefully acknowledge the data storage service SDS@hd supported by the Ministry of Science, Research and the Arts Baden-Württemberg (MWK) and the German Research Foundation (DFG) through grant INST 35/1314-1 FUGG. This work was supported by the European Research Council ERC-CoG-772395 (to J.S.); the German Research Foundation SFB/TRR152 (to D.B., J.S., and Y.S.) and SFB1158 (to K.S.-S., C.A., T.K., A.T.-T., and J.S.); an exploration grant by the Boehringer Ingelheim Foundation (to J.S.); SFB1134 (to T.K.); and a fellowship of the Physician Scientist Program of the Medical Faculty of Heidelberg (to G.B.K.). C.A. is supported by the Chica and Heinz Schaller Foundation and NARSAD.

Data and code availability

- Data: The datasets supporting the current study have not been deposited in a public repository but are available from the corresponding author upon request.
- Code: This paper does not report original code.
- Any additional information required to reanalyze the data reported in this paper is available from the lead contact upon request.

References

Allen WE, Denardo LA, Chen MZ, Liu CD, Loh KM, Fenno LE, Ramakrishnan C, Deisseroth K, Luo L. Thirst-associated preoptic neurons encode an aversive motivational drive. Science. 2017; 357: 1149–1155. [PubMed: 28912243]

Baker MA. A brain-cooling system in mammals. Sci Am. 1979; 240: 130–139. [PubMed: 451531]

Baldwin BA, Ingram DL. Effect of heating & cooling the hypo-thalamus on behavioral thermoregulation in the pig. J Physiol. 1967; 191: 375–392. [PubMed: 6050111]

Barbour HG. Die Wirkung unmittelbarer Erwärmung und Abkühlung der Wärmezentra auf die Körpertemperatur. Archiv für experimentelle Pathologie und Pharmakologie volume. 1912; 70: 1–26.

Boulant JA. Counterpoint: Heat-induced membrane depolarization of hypothalamic neurons: an unlikely mechanism of central thermosensitivity. Am J Physiol Regul Integr Comp Physiol. 2006; 290: R1481–R1484. [PubMed: 16708422]

Boulant JA, Dean JB. Temperature receptors in the central nervous system. Annu Rev Physiol. 1986; 48: 639–654. [PubMed: 3010828]

Cai DJ, Aharoni D, Shuman T, Shobe J, Biane J, Song W, Wei B, Veshkini M, La-Vu M, Lou J, et al. A shared neural ensemble links distinct contextual memories encoded close in time. Nature. 2016; 534: 115–118. [PubMed: 27251287]

Caterina MJ, Schumacher MA, Tominaga M, Rosen TA, Levine JD, Julius D. The capsaicin receptor: a heat-activated ion channel in the pain pathway. Nature. 1997; 389: 816–824. [PubMed: 9349813]

Chen TW, Wardill TJ, Sun Y, Pulver SR, Renninger SL, Baohan A, Schreiter ER, Kerr RA, Orger MB, Jayaraman V, et al. Ultrasensitive fluorescent proteins for imaging neuronal activity. Nature. 2013; 499: 295–300. [PubMed: 23868258]

Coman D, de Graaf RA, Rothman DL, Hyder F. In vivo three-dimensional molecular imaging with Biosensor Imaging of Redundant Deviation in Shifts (BIRDS) at high spatiotemporal resolution. NMR Biomed. 2013; 26: 1589–1595. [PubMed: 23881869]

Fenrich M, Habjanovic K, Kajan J, Heffer M. The circle of Willis revisited: Forebrain dehydration sensing facilitated by the anterior communicating artery: How hemodynamic properties facilitate more efficient dehydration sensing in amniotes. BioEssays. 2021; 43 e2000115 [PubMed: 33191609]

Ghosh KK, Burns LD, Cocker ED, Nimmerjahn A, Ziv Y, Gamal AE, Schnitzer MJ. Miniaturized integration of a fluorescence microscope. Nat Methods. 2011; 8: 871–878. [PubMed: 21909102]

Griffin JD, Kaple ML, Chow AR, Boulant JA. Cellular mechanisms for neuronal thermosensitivity in the rat hypothalamus. J Physiol. 1996; 492: 231–242. [PubMed: 8730598]

Guzman RE, Schwarz YN, Rettig J, Bruns D. SNARE force synchronizes synaptic vesicle fusion and controls the kinetics of quantal synaptic transmission. J Neurosci. 2010; 30: 10272–10281. [PubMed: 20685972]

Hammel HT. Regulation of internal body temperature. Annu Rev Physiol. 1968; 30: 641–710. [PubMed: 4871163]

Hammel HT, Hardy JD, Fusco MM. Thermoregulatory responses to hypothalamic cooling in unanesthetized dogs. Am J Physiol. 1960; 198: 481–486. [PubMed: 14399311]

Heller HC, Crawshaw LI, Hammel HT. The thermostat of vertebrate animals. Sci Am. 1978; 239: 102–110. [PubMed: 684402]

Hori T, Nakashima T, Kiyohara T, Shibata M, Hori N. Effect of calcium removal on thermosensitivity of preoptic neurons in hypothalamic slices. Neurosci Lett. 1980; 20: 171–175. [PubMed: 6255374]

Hu HZ, Gu Q, Wang C, Colton CK, Tang J, Kinoshita-Kawada M, Lee LY, Wood JD, Zhu MX. 2-aminoethoxydiphenyl borate is a common activator of TRPV1, TRPV2, and TRPV3. J Biol Chem. 2004; 279: 35741–35748. [PubMed: 15194687]

Jessen C. Thermal afferents in the control of body temperature. Pharmacol Ther. 1985; 28: 107–134. [PubMed: 4059328]

Jo A, Xu J, Deniz S, Cherian S, DeVries SH, Zhu Y. Intersectional Strategies for Targeting Amacrine and Ganglion Cell Types in the Mouse Retina. Front Neural Circuits. 2018; 12: 66. [PubMed: 30186122]

Kelso SR, Boulant JA. Effect of synaptic blockade on thermosensitive neurons in hypothalamic tissue slices. Am J Physiol. 1982; 243: R480–R490. [PubMed: 7137377]

Kelso SR, Perlmutter MN, Boulant JA. Thermosensitive single-unit activity of in vitro hypothalamic slices. Am J Physiol. 1982; 242: R77–R84. [PubMed: 7058933]

Kobayashi S, Takahashi T. Whole-cell properties of temperature-sensitive neurons in rat hypothalamic slices. Proc Biol Sci. 1993; 251: 89–94. [PubMed: 8096083]

Kobayashi S, Hori A, Matsumura K, Hosokawa H. Point: Heat-induced membrane depolarization of hypothalamic neurons: a putative mechanism of central thermosensitivity. Am J Physiol Regul Integr Comp Physiol. 2006; 290: R1479–R1480. [PubMed: 16603658]

Long MA, Fee MS. Using temperature to analyse temporal dynamics in the songbird motor pathway. Nature. 2008; 456: 189–194. [PubMed: 19005546]

Madden CJ, Morrison SF. Central nervous system circuits that control body temperature. Neurosci Lett. 2019; 696: 225–232. [PubMed: 30586638]

Magoun HW, Harrison F, Brobeck JR, Ranson SW. Activation of heat loss mechanisms by local heating of the brain. J Neurophysiol. 1938; 1: 101–114.

Mishra SK, Tisel SM, Orestes P, Bhangoo SK, Hoon MA. TRPV1-lineage neurons are required for thermal sensation. EMBO J. 2011; 30: 582–593. [PubMed: 21139565]

Moffitt JR, Bambah-Mukku D, Eichhorn SW, Vaughn E, Shekhar K, Perez JD, Rubinstein ND, Hao J, Regev A, Dulac C, Zhuang X. Molecular, spatial, and functional single-cell profiling of the hypothalamic preoptic region. Science. 2018; 362: 362.

Möhler H, Rudolph U. Disinhibition, an emerging pharmacology of learning and memory. F1000Res. 2017; 6: 6.

Morrison SF, Nakamura K. Central Mechanisms for Thermoregulation. Annu Rev Physiol. 2019; 81: 285–308. [PubMed: 30256726]

Mulier M, Vandewauw I, Vriens J, Voets T. Reply to: Heat detection by the TRPM2 ion channel. Nature. 2020; 584: E13–E15. [PubMed: 32788731]

Ota W, Nakane Y, Kashio M, Suzuki Y, Nakamura K, Mori Y, Tominaga M, Yoshimura T. Involvement of TRPM2 and TRPM8 in temperature-dependent masking behavior. Sci Rep. 2019; 9 3706 [PubMed: 30842533]

Perraud AL, Fleig A, Dunn CA, Bagley LA, Launay P, Schmitz C, Stokes AJ, Zhu Q, Bessman MJ, Penner R, et al. ADP-ribose gating of the calcium-permeable LTRPC2 channel revealed by Nudix motif homology. Nature. 2001; 411: 595–599. [PubMed: 11385575]

Peters JH, McDougall SJ, Fawley JA, Smith SM, Andresen MC. Primary afferent activation of thermosensitive TRPV1 triggers asynchronous glutamate release at central neurons. Neuron. 2010; 65: 657–669. [PubMed: 20223201]

Piatkevich KD, Bensussen S, Tseng HA, Shroff SN, Lopez-Huerta VG, Park D, Jung EE, Shemesh OA, Straub C, Gritton HJ, et al. Population imaging of neural activity in awake behaving mice. Nature. 2019; 574: 413–417. [PubMed: 31597963]

Pogorzala LA, Mishra SK, Hoon MA. The cellular code for mammalian thermosensation. J Neurosci. 2013; 33: 5533–5541. [PubMed: 23536068]

Roth BL. DREADDs for Neuroscientists. Neuron. 2016; 89: 683–694. [PubMed: 26889809]

Sabatini BL, Regehr WG. Timing of neurotransmission at fast synapses in the mammalian brain. Nature. 1996; 384: 170–172. [PubMed: 8906792]

Sano Y, Inamura K, Miyake A, Mochizuki S, Yokoi H, Matsushime H, Furuichi K. Immunocyte Ca2+ influx system mediated by LTRPC2. Science. 2001; 293: 1327–1330. [PubMed: 11509734]

Siemens J, Kamm GB. Cellular populations and thermosensing mechanisms of the hypothalamic thermoregulatory center. pflugers Arch. 2018; 470: 809–822. [PubMed: 29374307]

Song K, Wang H, Kamm GB, Pohle J, Reis FC, Heppenstall P, Wende H, Siemens J. The TRpM2 channel is a hypothalamic heat sensor that limits fever and can drive hypothermia. Science. 2016; 353: 1393–1398. [PubMed: 27562954]

Sukstanskii AL, Yablonskiy DA. An analytical model of temperature regulation in human head. J Therm Biol. 2004; 29: 583–587.

Tabarean I. Central thermoreceptors. Handb Clin Neurol. 2018; 156: 121–127. [PubMed: 30454585]

Tan CL, Cooke EK, Leib DE, Lin Y-C, Daly GE, Zimmerman CA, Knight ZA. Warm-Sensitive Neurons that Control Body Temperature. Cell. 2016; 167: 47–59. e15 [PubMed: 27616062]

Tan CL, Knight ZA. Regulation of Body Temperature by the Nervous System. Neuron. 2018; 98: 31–48. [PubMed: 29621489]

Tan CH, McNaughton PA. The TRpM2 ion channel is required for sensitivity to warmth. Nature. 2016; 536: 460–463. [PubMed: 27533035]

Ting JT, Daigle TL, Chen Q, Feng G. Acute brain slice methods for adult and aging animals: application of targeted patch clampanalysis and optogenetics. Methods Mol Biol. 2014; 1183: 221–242. [PubMed: 25023312]

Togashi K, Inada H, Tominaga M. Inhibition ofthe transient receptor potential cation channel TRPM2 by 2-aminoethoxydiphenyl borate (2-APB). Br J Pharmacol. 2008; 153: 1324–1330. [PubMed: 18204483]

Vandewauw I, De Clercq K, Mulier M, Held K, Pinto S, Van Ranst N, Segal A, Voet T, Vennekens R, Zimmermann K, et al. ATRP channel trio mediates acute noxious heat sensing. Nature. 2018; 555: 662–666. [PubMed: 29539642]

Vilar B, Tan CH, McNaughton PA. Heat detection by the TRpM2 ion channel. Nature. 2020; 584: E5–E12. [PubMed: 32788732]

Vishwakarma LC, Sengupta T, Jaryal AK, Mallick HN. Cortex senses environmental temperature earlier than the hypothalamus in awake rats. J Therm Biol. 2020; 91 102652 [PubMed: 32716856]

Vriens J, Owsianik G, Hofmann T, Philipp SE, Stab J, Chen X, Benoit M, Xue F, Janssens A, Kerselaers S, et al. TRPM3 is a nociceptor channel involved in the detection of noxious heat. Neuron. 2011; 70: 482–494. [PubMed: 21555074]

Wang XJ, Yang GR. A disinhibitory circuit motif and flexible information routing in the brain. Curr Opin Neurobiol. 2018; 49: 75–83. [PubMed: 29414069]

Watakabe A, Ichinohe N, Ohsawa S, Hashikawa T, Komatsu Y, Rockland KS, Yamamori T. Comparative analysis of layer-specific genes in Mammalian neocortex. Cereb Cortex. 2007; 17: 1918–1933. [PubMed: 17065549]

Xu SZ, Zeng F, Boulay G, Grimm C, Harteneck C, Beech DJ. Block of TRPC5 channels by 2-aminoethoxydiphenyl borate: a differential, extracellular and voltage-dependent effect. Br J Pharmacol. 2005; 145: 405–414. [PubMed: 15806115]

Yamamoto S, Shimizu S, Kiyonaka S, Takahashi N, Wajima T, Hara Y, Negoro T, Hiroi T, Kiuchi Y, Okada T, et al. TRPM2-mediated Ca2+influx induces chemokine production in monocytes that aggravates inflammatory neutrophil infiltration. Nat Med. 2008; 14: 738–747. [PubMed: 18542050]

Yang CF, Chiang MC, Gray DC, Prabhakaran M, Alvarado M, Juntti SA, Unger EK, Wells JA, Shah NM. Sexually dimorphic neurons in the ventromedial hypothalamus govern mating in both sexes and aggression in males. Cell. 2013; 153: 896–909. [PubMed: 23663785]

Yarmolinsky DA, Peng Y, Pogorzala LA, Rutlin M, Hoon MA, Zuker CS. Coding and plasticity in the Mammalian Thermosensory System. Neuron. 2016; 92: 1079–1092. [PubMed: 27840000]

Zhang Y, Pak C, Han Y, Ahlenius H, Zhang Z, Chanda S, Marro S, Patzke C, Acuna C, Covy J, et al. Rapid single-step induction of functional neurons from human pluripotent stem cells. Neuron. 2013; 78: 785–798. [PubMed: 23764284]

Zhang KX, D'Souza S, Upton BA, Kernodle S, Vemaraju S, Nayak G, Gaitonde KD, Holt AL, Linne CD, Smith AN, et al. Violet-light suppression of thermogenesis by opsin 5 hypothalamic neurons. Nature. 2020; 585: 420–425. [PubMed: 32879486]

Zhao Y, Boulant JA. Temperature effects on neuronal membrane potentials and inward currents in rat hypothalamic tissue slices. J Physiol. 2005; 564: 245–257. [PubMed: 15695248]

Zhou P, Resendez SL, Rodriguez-Romaguera J, Jimenez JC, Neufeld SQ, Giovannucci A, Friedrich J, Pnevmatikakis EA, Stuber GD, Hen R, et al. Efficient and accurate extraction of in vivo calcium signals from microendoscopic video data. eLife. 2018; 7: 7.

Europe PMC Funders Author Manuscripts

Highlights

- Temperature in the hypothalamic preoptic area (POA) tracks body temperature in mice
- TRPM2 participates in warmth detection in the POA *in vivo*
- Presynaptic TRPM2 detects temperature increases to activate warm-sensitive neurons
- Warming enhances inhibitory transmitter release via TRPM2 to mediate disinhibition

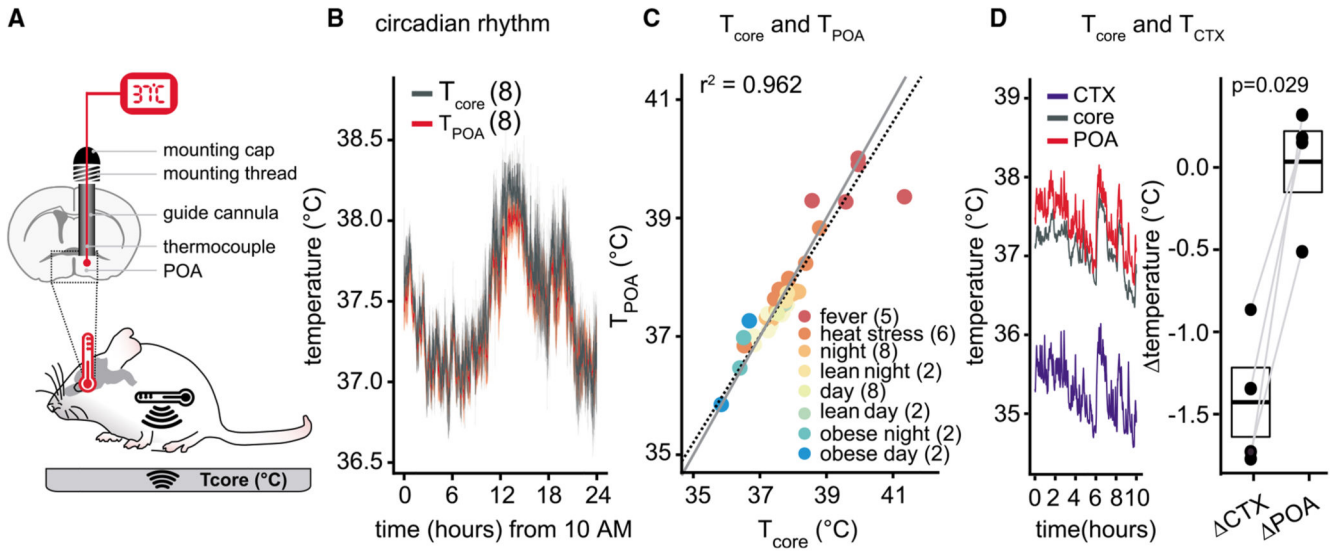

Figure 1. POA temperature precisely tracks body temperature

(A) Scheme showing the methodology used to measure body and POA temperatures (T_{core} and T**POA**, respectively) in freely moving mice.

(B) T_{core} and T**POA** were measured during 24 h in C57BL/6N mice (mean ± SEM).

(C) Relationship between T_{core} and T**POA** underdifferent conditions. Each dot represents an individual mouse. Datawere fitted to a linear model (dotted line), and theoretical y = x line equation is plotted in gray.

(D) Left: measurements of T_{core}, T**POA**, and cortex temperature (T_{CTX}) in a representative freely moving C57BL/6N mouse. Right: boxplot showing the difference between T_{core} and T_{CTX} (ΔCTX) and T_{core} and T_{POA} (ΔPOA; mean ± SEM; Mann Whitney test; n = 4). Number of mice per experimental group is indicated in brackets.

See also Figure S1 and Table S1.

Europe PMC Funders Author Manuscripts

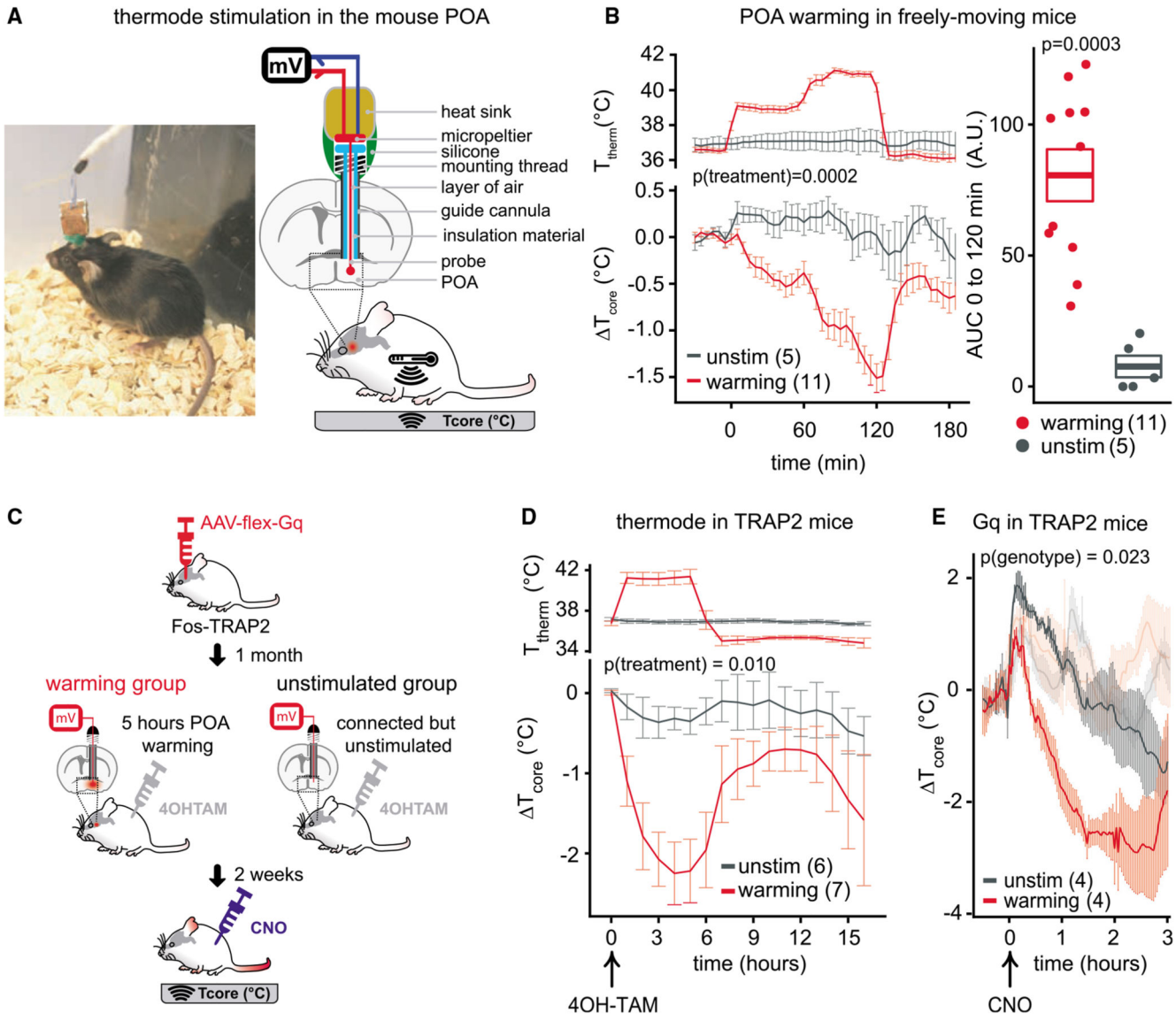

Figure 2. POA warming triggers a heat loss response that can be reactivated in Fos-TRAP2 mice

(A) Picture (left) and scheme (right) depicting the thermode used to manipulate brain temperature in freely moving mice. Stimulation temperatures (T_{therm}) were measured with a thermocouple fixed 1 mm from the tip of the thermode (not shown in the scheme). Body temperature (T_{core}) was recorded telemetrically.

(B) Left: T_{therm} and ΔT_{core} traces ofthermode-stimulated (red, warming) orthermode-connected but not stimulated (black, unstim) C57BL/6N mice (two-way RM ANOVA). Right: boxplot showing the area underthe curve (AUC) of individual traces shown in the left panel during POA warming (from 0 to 120 min; two-tailed t test).

(C) Experimental approach using Fos-TRAP2 mice.

(D) Average ΔT_{core} and T_{therm} in Fos-TRAP2 mice that were intraperitoneally (i.p.) injected with 4OH-tamoxifen (50 mg/kg) just before POA stimulation (red, warming) or no stimulation (black, unstim; two-way RM ANOVA).

Europe PMC Funders Author Manuscripts

(E) Changes in T_{core} upon CNO (0.3 mg/kg, foreground traces) or vehicle (saline, background traces) i.p. injections in thermode-stimulated (red) or -unstimulated (black) Fos-TRAP2 mice expressing Gq-DREADD in preoptic neurons (two-way RM ANOVA). See also Figures S1 and S2 and Table S1. Data represent mean ± SEM.

Europe PMC Funders Author Manuscripts

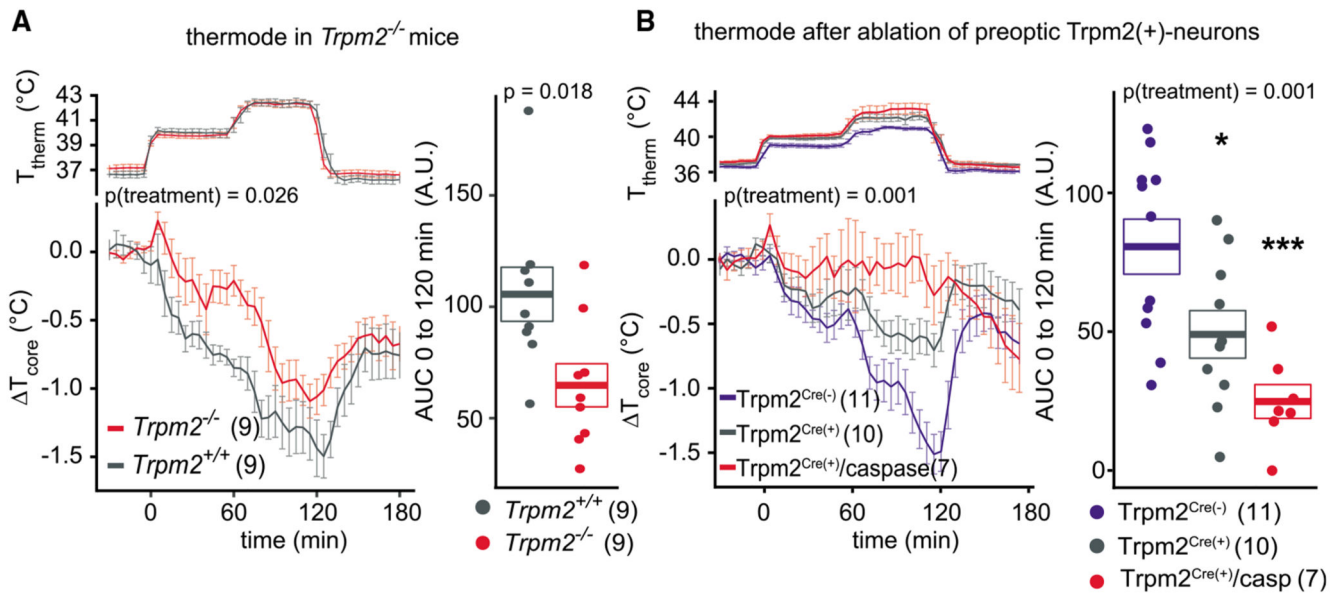

Figure 3. TRPM2 participates in temperature detection in the POA

(A) Left: changes in T_{core} and T_{therm} upon two steps of POA warming in *Trpm2*$^{-/-}$ (red) and littermate controls (black, *Trpm2*$^{+/+}$; two-way RM ANOVA). Right: boxplot showing the AUC of individual traces shown in the left panel during POA warming (from 0 to 120 min; two-tailed t test).

(B) Left: changes in T_{core} and Ttherm upon two steps of POA warming in Cre-expressing Trpm2$^{Cre(+)}$ (black) and Cre-negative Trpm2$^{Cre(-)}$ (blue) and littermate Trpm2$^{Cre(+)}$-ablated (red) mice (two-way RM ANOVA). Right: boxplot showing theAUC of individual traces shown in the left panel during POA warming (from 0 to 120 min; one-way ANOVA followed by Newman-Keuls post test. **p < 0.01, ***p < 0.05). Number of mice per experimental group is indicated in brackets. Note: stimulated Trpm2$^{Cre(-)}$ animals in Figure 3B correspond to the same cohort also shown in Figure 2B.

See also Figures S2 and S3 and Table S1. Data represent mean ± SEM.

Europe PMC Funders Author Manuscripts

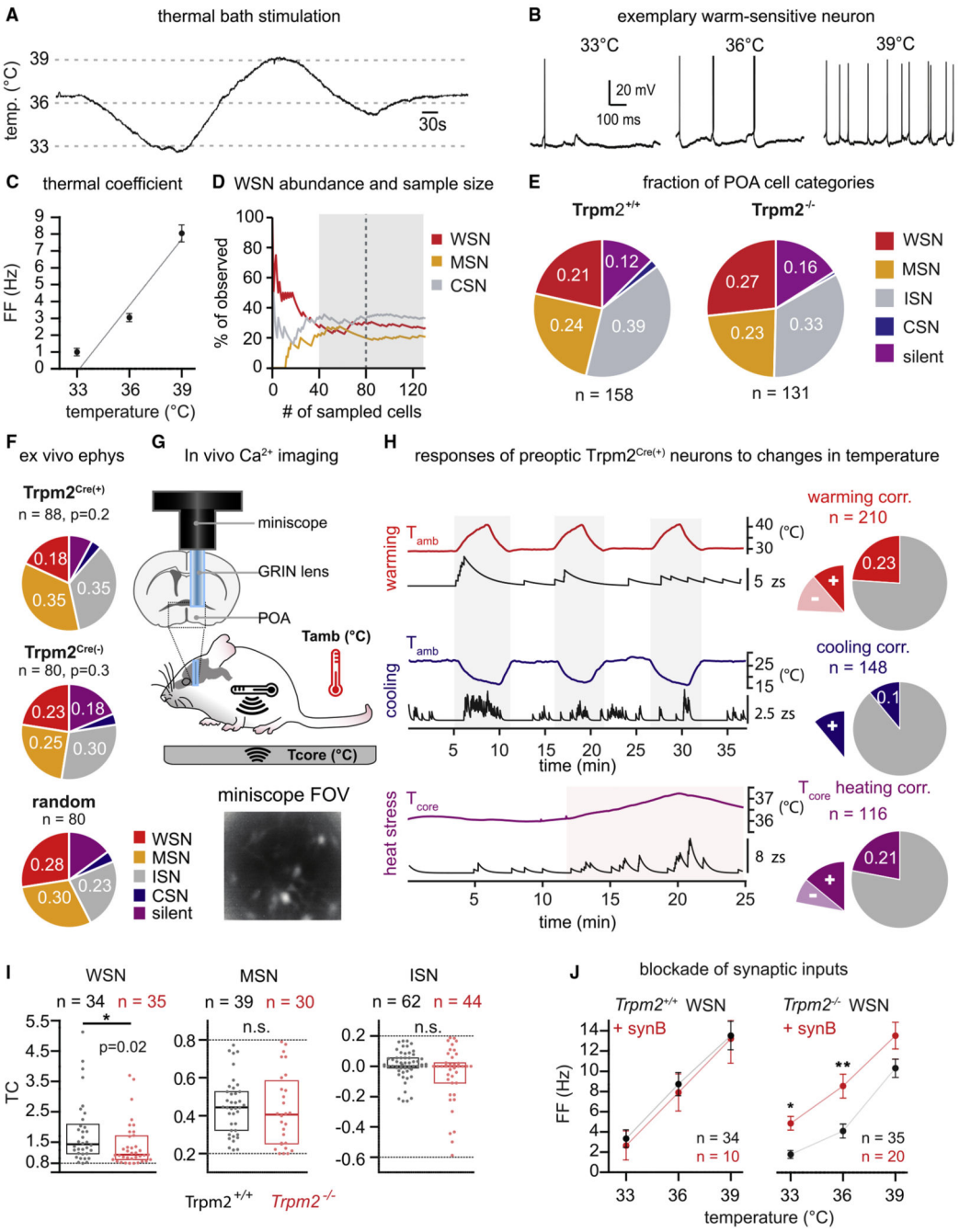

Figure 4. TRPM2 enhances temperature sensitivity of WSNs

(A) Representative trace of the sinusoidal temperature stimulus applied to acute POA slices.

(B) Representative trace of the action potential (AP) firing patterns as a function of chamber temperature recorded from a POA WSN.

(C) Linear fit of the AP frequency recordings obtained from the WSN depicted in (B) as a function of temperature (mean ± SEM).

(D) Proportion of cell categories as a function of sample size obtained in whole-cell patch-clamp recordings.

(E) Distribution of POA cell categories based on their electrophysiologically recorded temperature sensitivities obtained from *Trpm2*$^{+/+}$ (left) and *Trpm2*$^{-/-}$ (right) slices. Warm-sensitive neuron (WSN), moderately warm-sensitive neuron (MSN), temperature-insensitive neuron (ISN), cold-sensitive neuron (TC < -0.6; CSN), and silent neuron firing no APs (silent) are shown.

(F) Electrophysiological recordings of Trpm2$^{Cre(+)}$, Trpm2$^{Cre(-)}$, and randomly sampled neurons in acute POA brain slice preparations. Total number of sampled cells (n) and the p values corresponding to a chi-square test are depicted next to the pie charts.

(G) Scheme of implanted GRIN lens and miniscope used for POA imaging in freely moving mice are shown together with a representative field of view (FOV).

(H) Left: warming-correlated (top), cooling-correlated (middle), and body-temperature-correlated (bottom) calcium traces from GCaMP6s-positive neurons detected in the POA of Trpm2$^{Cre(+)}$ mice (6, 6, and 5 mice, respectively); response magnitudes are *Z* scored (zs). T_{amb}, ambient temperature. Right: pie charts indicating the proportions of correlated neurons responding to the corresponding temperature challenges.

(I) Temperature coefficients (TCs) deduced from linear fits of all electrophysiologically recorded WSNs, MSNs, and ISNs of *Trpm2*$^{+/+}$ (black) or *Trpm2*$^{-/-}$ (red) POA slices. Median (thick line) and interquartile range (box) with scatterplot of individual datapoints are shown. Dashed lines demarcate the TC cutoffs for each corresponding cell category.

(J) AP frequency versus bath temperature plot (mean ± SEM) for all recorded *Trpm2*$^{+/+}$ (left) or *Trpm2*$^{-/-}$ (right) WSNs in the presence (red) or absence (black) of a cocktail of synaptic blockers (+synB) containing 10 μM CNQX, 50 μM D-AP5, and 20 μM SR-95531 (Gabazine or SR). *p < 0.05, **p < 0.005, Dunn's test); n, total number of sampled cells in each genotype and treatment group.

See also Figures S4 and S5 and Table S1.

Europe PMC Funders Author Manuscripts

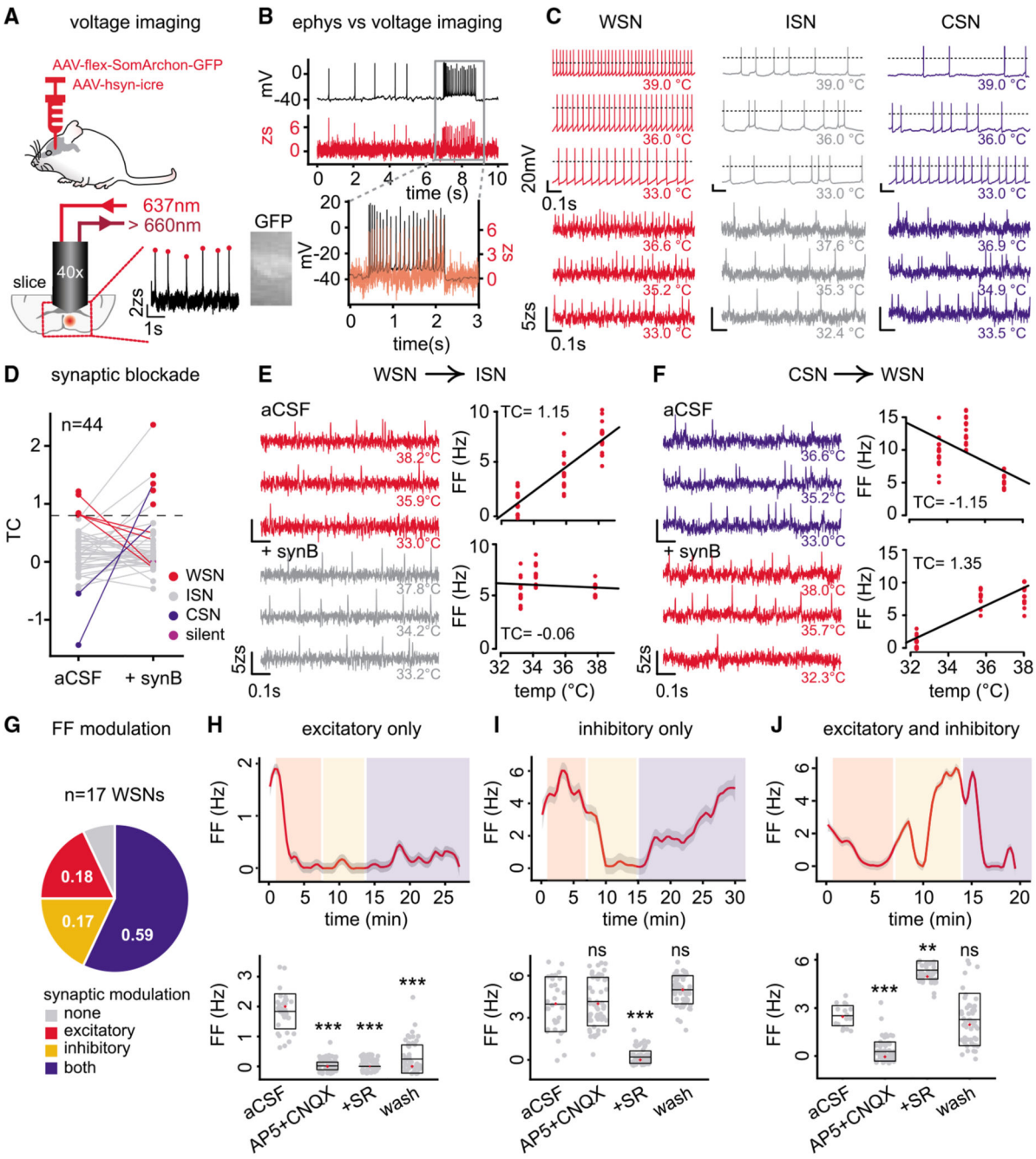

Figure 5. Synaptic input robustly modulates temperature sensitivity of POA neurons

(A) Experimental methodology used to visualize changes in membrane voltage in acute mouse brain slices using the genetically encoded voltage indicator SomArchon.

(B) Changes in SomArchon fluorescence (red; zs, *Z* score) and simultaneously recorded membrane voltage using whole-cell patch-clamp (black) in a preoptic neuron visualized using GFP.

(C) Representative AP firing patterns as a function of chamber temperature of preoptic WSNs (red), ISNs (gray), and CSNs (blue) using whole-cell patch clamp (top) or voltage

imaging (bottom) in acute mouse brain slices. Bath temperature is indicated below each trace.

(D) Temperature coefficient (TC) of randomly recorded preoptic neurons expressing SomArchon during baseline (aCSF) and after the application of a synaptic blocker cocktail (+synB: 10 μM CNQX, 50 μM D-AP5, and 20 μM SR-95531); dashed line demarcates TC cutoff for WSNs; n, total number of sampled cells.

(E and F) Representative traces of AP firing patterns and firing frequencies (FFs) as a function of chamber temperature recorded in a preoptic WSN (E) and a CSN

(F) before (aCSF) and after application of synB. FF as function of bath temperature was linearly fitted (black line) to calculate TC. Dots showing the FF have been jittered for better visualization.

(G) Fraction of WSNs that show modulation of their FFs by excitatory inputs, inhibitory inputs, or both during the bath application of CNQX + D-AP5 and CNQX + D-AP5 + SR (+SR condition) at 33°C. WSNs that changed their FF significantly during the application of CNQX and D-AP5 were classified as modulated by excitatory inputs, and those that only changed their FF during the subsequent wash in of SR were classified as modulated by inhibitory inputs and modulated by both if their FF changed during the first and second application of synaptic blockers.

(H-J) FFs of exemplary WSNs quantified in (G). Top: FFs of representative preoptic WSNs that changed their FFs during blockade of glutamatergic inputs (H), GABAergic inputs (I), or both (J). Pink-shaded areas indicate the application of CNQX and D-AP5, and yellow-shaded areas indicate the application of CNQX, D-AP5, and SR. The white and blue areas indicate baseline and wash-out periods, respectively. Bottom: boxplots show the quantification of traces shown in top panel (box, mean ± 2SD; red dot, median; Kruskal-Wallis followed by Bonferroni post test. $^{**}p < 0.01$, $^{***}p < 0.001$).

Europe PMC Funders Author Manuscripts

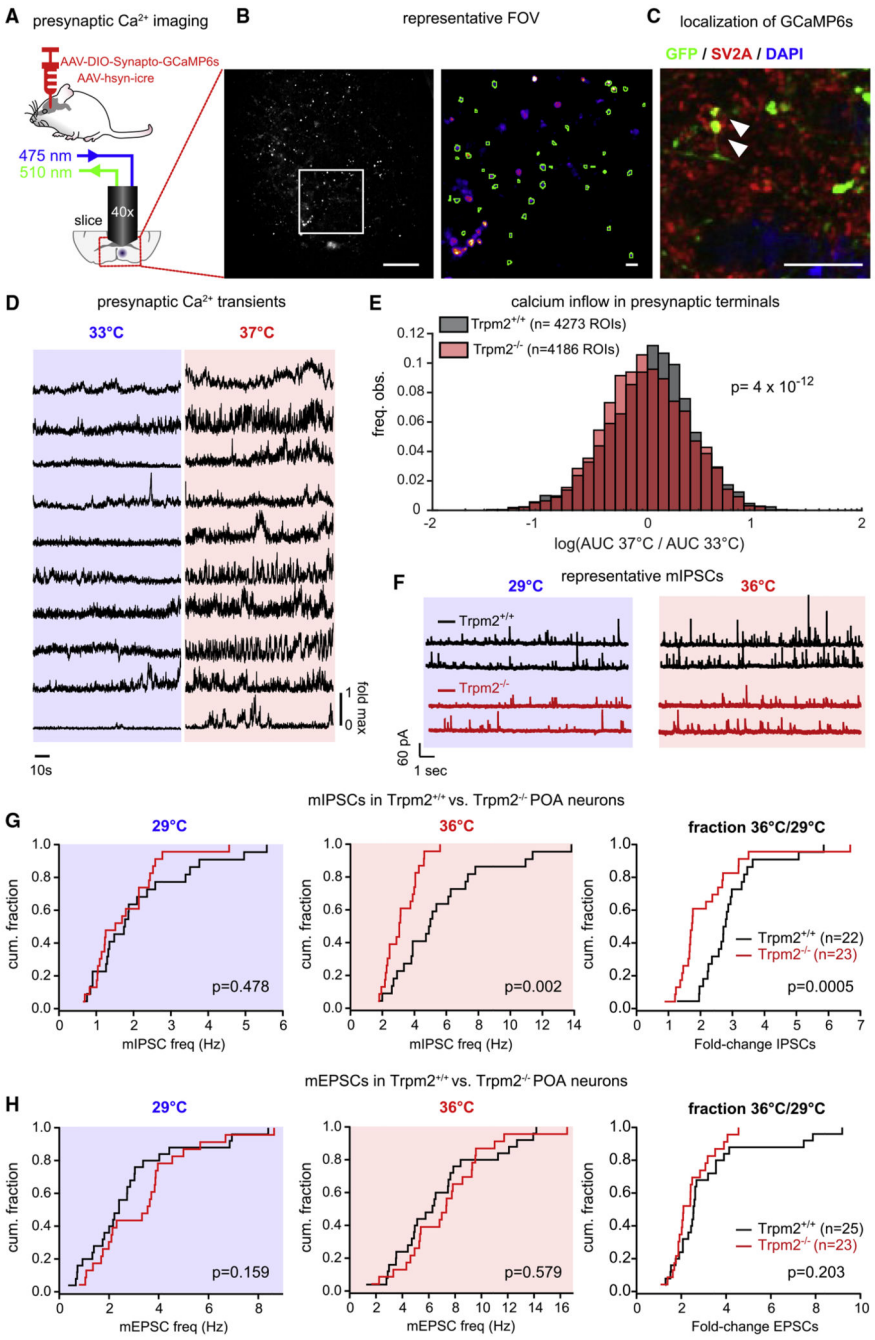

Figure 6. TRPM2 enhances calcium influx into presynaptic terminals and boosts inhibitory postsynaptic currents in a temperature-dependent manner

(A) Cartoon depicting the strategy to perform calcium imaging in presynaptic terminals using the synaptophysin-fused GCaMP6s (synapto-GCaMP6s) calcium indicator.

(B) Left: representative FOV of synapto-GCaMP6s expressing POA brain slices. Scale bar, 50 μm. Right: magnification of the area depicted in the left panel; regions of interest are shown in green. Scale bar, 5 μm.

(C) Representative immunohistochemical labeling of POA brain slices showing the expression of synapto-GCaMP6s (green) and the synaptic marker gene SV2A (red); arrowheads indicate double labeling. Scale bar, 10 μm.
(D) Representative traces showing increasing calcium activity in POA axonal terminals when temperature is shifted from 33°C to 37°C.
(E) Histogram showing the ratios of the area under the curve (AUC) of the ΔF/F0 traces recorded at 37°C and 33°C during equal time intervals of at least 100 s from *Trpm2*$^{+/+}$ and *Trpm2*$^{-/-}$ terminals.
(F) Representative mIPSCs observed at two different temperatures in *Trpm2*$^{+/+}$ (black) and *Trpm2*$^{-/-}$ (red) POA neurons.
(G and H) Cumulative plots of mIPSC (G) and mEPSC (H) frequencies detected in POA neurons from *Trpm2*$^{+/+}$ (black) and *Trpm2*$^{-/-}$ (red) mice at the indicated temperatures. Number of experimental units is indicated in brackets.
See also Figures S7-S9 and Table S1.

Europe PMC Funders Author Manuscripts

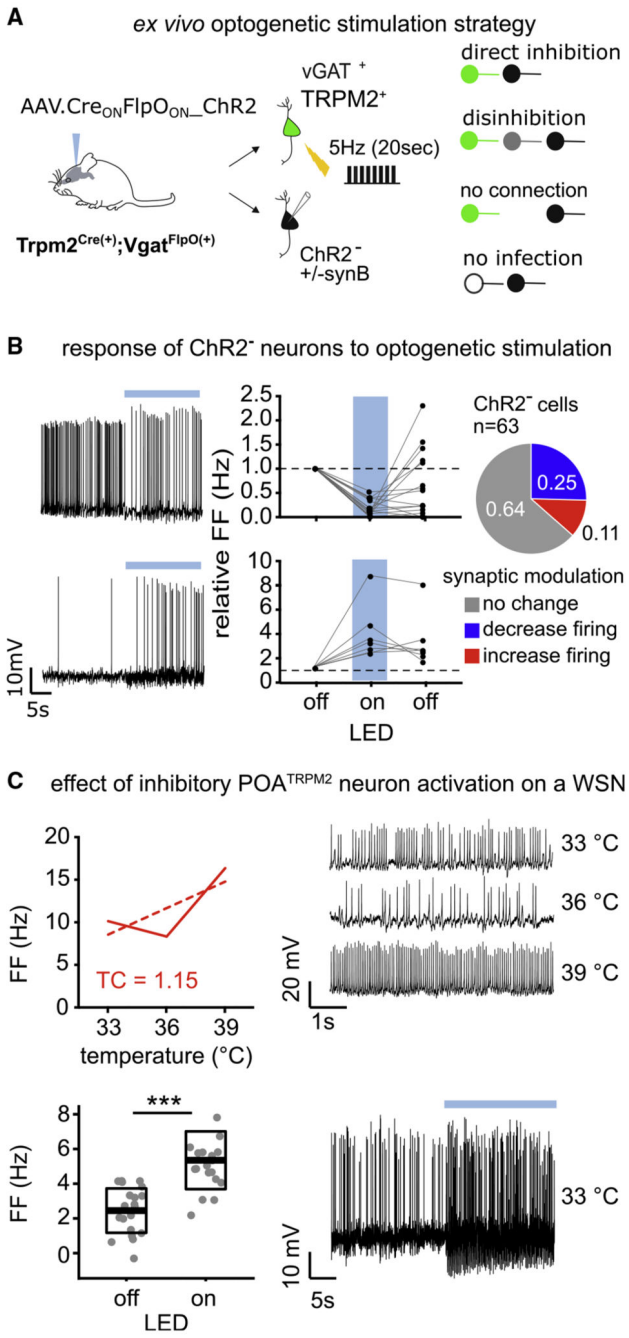

Figure 7. WSN activity is modulated by POA^{Trpm2} neurons

(A) Left: cartoon depicting Cre- and FlpO-dependent ChR2 expression strategy for optogenetic stimulation of GABAergic TRPM2-expressing neurons in POA slices. The firing frequency of randomly selected ChR2-negative (ChR2$^-$) POA neurons was recorded before, during, and after light activation (5 Hz, 20 s). At the end of each recording, the effect of synaptic blockers on light-induced firing wastested bythe sequential application ofCNQX/AP5 followed by a mix containing CNQX/AP5/Gabazine. Right: possible connectivity scenarios.

(B) Left: representative traces and corresponding firing frequency plots of two example neurons that show a light-induced firing frequency (FF) decrease or increase, respectively. Middle: quantification of traces shown in the left panel. Blue bars denote light stimulation. Right: proportions of randomly sampled ChR2^{-} POA neurons showing FF modulation upon optogenetic activation of GABAergic TRPM2-expressing neurons.

(C) Top left: FF as function of chamber temperature and calculated TC; dotted line, linear regression. Top right: representative FF recordings to determine TC of WSN shown in the left panel. Bottom right: effect of optogenetic stimulation (blue bar) of TRPM2-expressing neurons on the firing frequency of a WSN. Bottom left: quantification of FF changes shown on the right.

See also Figure S10 and Table S1.

Europe PMC Funders Author Manuscripts